R/D.2827-EN

ELECTRO-OPTICAL TRANSMISSION AND LIQUID WATER CONTENT OF FOGS AND CLOUDS.

FINAL TECHNICAL REPORT

S. G. JENNINGS

MAY 1985

European Research Office
United States Army Research, Development
and Standardization Groups - UK
223-231 Marylebone Road
London NW1, England.

Contract Number DAJA37-81-C-0003

University College Galway

DISCLAIMER NOTICE

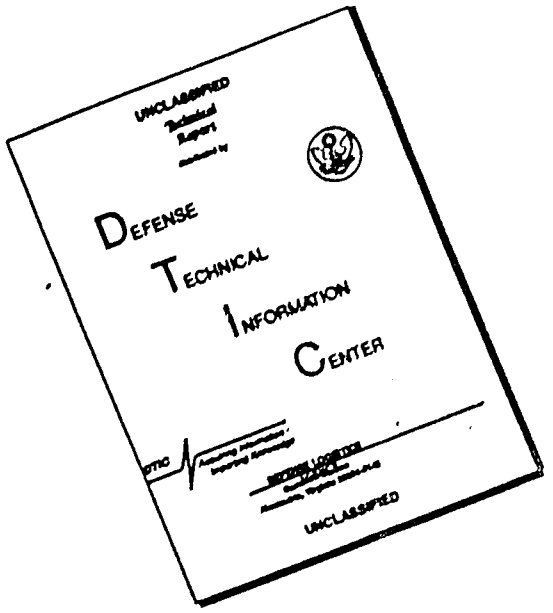

THIS DOCUMENT IS BEST QUALITY AVAILABLE. THE COPY FURNISHED TO DTIC CONTAINED A SIGNIFICANT NUMBER OF PAGES WHICH DO NOT REPRODUCE LEGIBLY.

The views, opinions and findings contained in this report are those of the author and should not be construed as an official Department of the Army position, policy, or decision unless so designated by other documentation.

ABSTRACT

Simultaneous measurement of the extinction coefficient σ_e and liquid water content W were made for laboratory generated cloud at CO_2 laser wavelength λ = 10.591 micrometres (μm). Good agreement between measurement and prediction (Chýlek, 1978) was found for a wide range of W (up to 7 g m^{-3}) and σ_e (up to 1 m^{-1}).

The first definitive measurements of backscatter, σ_b, and extinction coefficients made on laboratory - generated fog droplet distributions at visible (λ = 0.6328 μm) wavelengths were in good agreement with a size distribution independent relation $\sigma_e = 17.7\ \sigma_b$ (Pinnick, Jennings et al, 1983).

The first definitive measurements of backscatter coefficient and extinction coefficient made on laboratory cloud are reported at CO_2 Laser wavelengths. The measurements yielding σ_e/σ_b ratios of between 350 and about 550 are in good agreement with numerical calculations performed on narrow size distributions of natural cloud.

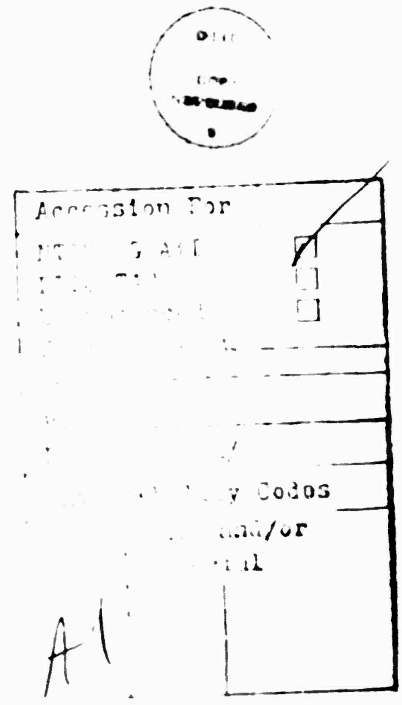

TABLE OF CONTENTS

CAPTIONS TO FIGURES

Fig. 1.1 Schematic diagram of optical arrangement used in the extinction coefficient measurements.

Fig. 1.2 A printout of histogram of droplet size distribution from cloud nebulizer generator.

Fig. 1.3 Measured laboratory-generated cloud droplet size distribution.

Fig. 1.4 LWC measurement system-direct filtration.

Fig. 1.5 LWC measurement system.

Fig. 1.6 Optical depth as a function of transmission path length in the laboratory cloud chamber.

Fig. 1.7 Measured values of extinction coefficient $\sigma_e(m^{-1})$ and of liquid water content $W(gm^{-3})$ for laboratory cloud at wavelength λ=10.591μm.

Fig. 1.8 Continuous simultaneous measurements of σ_e and W for laboratory cloud at λ=10.591 μm.

Fig. 1.9 Continuous simultaneous measurements of σ_e and W for laboratory cloud at λ= 10.591μm.

Fig. 2.1 Mie theory response calculations for the Knollerberg CSASP particle counter for NaCl particles (lighter curve) and water droplets.

Fig. 2.2 Volume extinction coefficient at a wavelength λ= 10.6μm versus liquid water content for 156 cloud droplet size distribution measurements of cumulus and stratus clouds.

Fig. 2.3 Variation of extinction coefficient with liquid water content in atmospheric fog and haze for 320 size distribution measurements made at different geographic locales and under a variety of meteorological conditions.

CAPTIONS TO TABLES

STATEMENT OF RESEARCH PROBLEM

Research conducted during the term of this contract consisted of measurement of transmission and backscatter of electromagnetic (em) energy through water droplet clouds with known size distribution and liquid water content at visible and infra-red (IR) wavelengths. Theoretical analyses of relations between extinction, absorption and backscatter which incorporate size distribution dependencies were also made.

SUMMARY OF MOST IMPORTANT RESULTS

Experimental measurements made of extinction coefficient σ_e, m^{-1} and liquid water content W, g m^{-3} for laboratory generated cloud at the CO_2 laser wavelength λ = 10.591 micrometres (μm) verified the size distribution independent relation $\sigma_e/W = 3\pi c/2\lambda$ derived by Chýlek (1978). The first continuous set of measurements of σ_e and W are reported.

The first definitive simultaneous set of measurements of volume backscatter and extinction coefficients σ_b,σ_e for laboratory cloud at visible wavelengths (λ = 0.6328 μm) are reported. The measurements show good agreement with the theoretically predicted size distribution independent relation:

$\sigma_e/\sigma_b = 8\pi/g(\lambda)$, (Pinnick et al, 1983), where g (λ) is a slowly varying function of wavelength.

The first definitive set of measurements of volume backscatter coefficient σ_b and volume extinction coefficient σ_e for laboratory generated cloud at CO_2 Laser wavelengths (10.261 - 10.591 μm) are reported. The measurements of extinction to backscatter ratio σ_e/σ_b possessing values ranging from 350 upward give relatively good agreement with numerical calculations carried out on relatively narrow size distributions for cumulus and stratus cloud (Pinnick et al, 1983).

LIST OF PUBLICATIONS AND PRESENTATIONS

Publications

Pinnick, R.G., S.G. Jennings, P. Chýlek, C. Ham and W.T. Jr. Grandy, 1983 "Backscatter and Extinction in Water Clouds." J. Geophy. Res., 88, 6787-6796.

Jennings, S.G., 1983, "Extinction and Liquid Water Content of Fog at Visible Wavelengths", Applied Optics, 22, 2514-2515.

Published Proceedings

Jennings, S.G., Pinnick, R.G., Chýlek, P. and Ham, C.V., 1982, "The relation between Backscatter and Extinction for Water Clouds". Proceedings of the Annual Conference on Remote Sensing and the Atmosphere, Remote Sensing Society, University of Reading, p.67, December 1982.

Jennings, S.G., Pinnick, R.G., and Grandy, W.T., Jr., 1984. "Backscatter and Extinction in Water Clouds", Proceedings of the 9th International Cloud Physics Conference, Tallinn, Estonian SSR, USSR; Vol.III, pp. 667-680.

Jennings, S.G., Pinnick, R.G., Chýlek, P., Auvermann, H.J. and Ham, C.V., 1980, "Relationships between IR Extinction, Absorption, Backscatter and Liquid Water Content of the Major Cloud Types" Proceedings of the VIII International Cloud Physics Conference, Clermount-Ferrand, France, pp.329-332, July 1980.

Presentations at Scientific Meetings

Jennings, S.G., Pinnick, R.G., Chýlek, P., and Ham, C.V., 1980, "Backscatter and Extinction in Water Clouds", 10th International Laser Radar Conference, University of Maryland, USA, October 1980.

Jennings, S.G., Pinnick, R.G., and Grandy, W.T., 1983. "Measurements of Backscatter and Extinction in Water Clouds". CSL Conference on Obscuration and Aerosol Research, Edgewood, Maryland, USA, June 1983.

PARTICIPATING SCIENTIFIC PERSONNEL

Principal Investigator: S.G. Jennings

Research Assistants: Dominic Herity, B.Sc.
Kathryn McCarthy, B.Sc.

Research Students: Margaret Naughton, B.Sc.
Peter F. Nolan, M.Sc., B.Sc.

P. Nolan's Ph.D. thesis title: Propagation of Electromagnetic Radiation through water clouds - being submitted for examination to the National University of Ireland, July 1985.

1. Electro-Optical Transmission and Liquid Water Content of Fogs and Clouds.

1.1. Introduction:

A possible relation between extinction and liquid water content is of considerable interest and has preoccupied atmospheric scientists over the past several decades. The determination of simple relationships between electro-optical (E-O) transmission and measureable meteorological parameters such as cloud water content (LWC) could be used to predict transmission at middle infrared (IR) wavelengths from a knowledge of cloud or fog LWC. Conversely, a measure of the transmission at middle IR wavelengths could yield a value of liquid water content using validated relations from this work.

Most previous work has been directed towards seeking relationships between liquid water content and visibility, for example:
Eldridge (1966, 1971), Barteneva and Polyakova (1965) and Kumai (1973). Pinnick et al (1978) give approximate empirical relationships between extinction coefficient σ_e and liquid water content W based on the work of the forementioned authors. However, Pinnick et al (1978) found that the predicted values of visible extinction σ_e differed by about an order of magnitude for the same LWC (0.01 g m^{-3}). Thus any size-distribution - independent relation between extinction at visible wavelengths and LWC cannot be applied to fogs in general.

1.2. Extinction, Absorption and Liquid Water Content of Water Clouds

Consider a polydispersion of spherical water droplets described by the size distribution n(r), where r is the radius of a given droplet. We examine relationships between the extinction, σ_e, absorption coefficients, σ_a, and the liquid water content W given by

$$\sigma_e = \int \pi r^2 Q_e(m,x) n(r) dr \qquad (1.1)$$

$$\sigma_a = \int \pi r^2 Q_a(m,x) n(r) dr \qquad (1.2)$$

$$W = \frac{4}{3} \pi \rho \int r^3 n(r)\, dr \qquad (1.3)$$

where ρ the liquid droplet density, Qe (m,x), Qa (m,x) are the efficiency factors for extinction and absorption for a droplet with refractive index m and size parameter x, defined by the ratio of the droplet circumference to radiation wavelength λ. It has been shown by Chýlek (1978) that the

efficiency factor Qe (m,x) can be approximated by a linear function of droplet size parameter

$$Q_e\ (m,x) = c\ (\lambda)\ x \qquad (1.4)$$

providing size parameter $x \leq x_m$ ($x_m = 2\pi r_m/\lambda$). Pinnick et al (1979) have also shown that

$$Q_a\ (m,x) = c^1(\lambda)\ x \qquad (1.5)$$

The use of these simple linear relationships for the Mie efficiency factors in the expressions for the extinction and absorption coefficients given by Eqs.(1) and (2) reduce these coefficients to the simple form:

$$\sigma_e = \frac{3\pi c}{2\lambda\rho}\ W \qquad (1.6)$$

$$\sigma_e = \frac{3\pi c^1}{2\lambda\rho}\ W \qquad (1.7)$$

where c (λ) and c^1 (λ) are the slopes of the straight lines approximating the Mie efficiency curves.

The wavelength at which these linear relationships are valid is determined by the radius of the largest droplets present in the polydispersion. Chýlek (1978) and Pinnick et al (1979) give values of the maximum radius r_m and corresponding wavelengths λ, required for the validity of (6) and (7). They find that the relation (6) should work best for water droplets in fog or cloud at or near λ = 11 μm where r_m is found to be 14 μm. However, relation (6) might also be expected to work reasonably well for fog or cloud droplets for the wavelength range $9.5 < \lambda \leq 11$ μm since $12.5 < r_m < 14$ μm at these wavelength values. One might expect relation (6) to work reasonably well even if droplets in a particular distribution have radii greater than 14 μm providing they do not contribute excessively to either the liquid water content or the extinction.

Pinnick et al. (1979) verified theoretically relation (6) within a factor 2 at λ = 11 μm for 341 droplet size distribution measurements of atmospheric fogs formed under a variety of meterological conditions, and for which reliable fog data was available. Pinnick et al. (1979) used the raw size distribution fog data of Pinnick et al., (1978), Garland (1971), Garland et al., (1973), Roach et al. (1976), Kunkel (1971), and Kumai (1973) to calculate the liquid water content and the extinction coefficient for all of the fogs, and compared the results to the theoretical relation (6).

One of the objectives of the work was to investigate experimentally the validity of relation (6) i.e, $\sigma_e = \frac{3\pi c}{2\lambda\rho}$. W by making simultaneous measurements of

(a) the extinction coefficient σ_e

(b) the liquid water content W

and (c) the size distribution of the droplets.

This approach is distinctly different from that of Pinnick et al (1979) in that the extinction coefficient and LWC is measured, rather than calculated from the drop size distributions. One reason for measuring the droplet size distribution is that the validity of relation (6) requires droplets must be less than a certain size as discussed earlier in 1.2.

1.3. Experimental Apparatus and Techniques

A 1 m^3 chamber of path length L = 1m, constructed of waterproof plywood was used for all measurements. The chamber walls were painted matt black to minimize stray light reflections. Saturation of the chamber was maintained through the use of matt black absorbing cloth material lining the chamber walls. A 5 cm diameter opening at the front side of the chamber permitted the entrance of laser radiation (either a He-Ne or Co_2 laser beam) into the chamber and also allowed for the extraction of backscattered light from the cloud droplets in the chamber. The laser beam traversed the chamber path length and emerged through a small aperture (few mm diameter) in the rear exit wall of the chamber

Figure 1.1. is a schematic diagram of the optical arrangement used in the extinction coefficient measurements. It consists of a tunable vertically polarised CO_2 laser source (Sylvania Model 941S) with wavelengths available over the wavelength range 10.2 to 10.7 micrometres (μm). The CO_2 laser transmissions path is made coincident with a visible (0.6328 μm) He-Ne laser transmission path. Alignment is accomplished with aluminized mirrors which are mounted on micrometer-controlled translational and rotational stages. A portion of the CO_2 laser beam is reflected by a ZnSe window for a laser reference signal. The main beam enters the fog/cloud chamber of pathlength L through a narrow window and exits through a second narrow window into a second dectector. The main beam and reference detectors (Laser Precision Corporation Models RkP-545 and Rk-5100) consist of a pyroelectric laser probe together with a synchronous radiometer readout. The synchronous ratiometer readout, model Rk-5200 is used for the output of the ratio of the main beam and reference signals. The detectors have negligible drift (about 10^{-6} W cm^{-2} after warm-up) compared to typical radiance levels monitored by the detectors

(of the order of 1 W cm^{-2}). The radiation wavelength is monitored precisely with a spectrum analyzer (Optical Engineering Inc. Model 16-A CO_2 Laser Spectrum Analyzer).

Appropriate consideration is given to optimum transmissometer design to reduce forward scattering corrections - in accordance with the results of Deepak and Box papers a, b, (1978). For example, the use of a 10 cm lens which focuses the CO_2 beam of half width 2.5 mm through an aperture of radius 0.5 mm will result in a correction of less than 2% due to forward scattering at λ = 10.6 μm for a Deirmendjian haze M (broad distribution) of mean droplet radius 5 μm. In this work, aperture diameters from 1 to 2.5 mm were used. Water droplet clouds were generated within the chamber by a pair of commercially available "cool-mist vapourizers". The cloud droplet size distribution was determined by a Particle Measuring Systems (PMS) classical scattering aerosol spectrometer probe (CSASP) which can sense water droplets with radii from 0.23 to 14 μm (Pinnick and Auvermann, 1979). Corrections were applied to the measured droplet size distributions in accordance with the response calculations for the Knollenberg light-scattering CSASP counter (Pinnick and Auvermann, 1979). The cloud generator covered the range of droplet sizes usually encountered in natural cloud. The cloud generally attained a steady state condition as indicated by the individual spectra measured over a period of five minutes. Narrower droplet spectra, predominantly in the radius range 0.3 to 3.4 μm were generated by a De Vilbiss model 65 ultrasonic nebulizer with fixed frequency 1.35 MHz and a water content output variable up to 6 g of water per minute. A typical sequence of histogram giving the number of drops per channel for size range 0 of the CSASP light scattering counter, is shown in Figure 1.2 for the cloud nebulizer generator. It can be seen that the mode radius lies in channel 5 corresponding to a droplet radius in the range 3.8 to 4.8 μm.

Water droplet clouds were also generated by a combination of a pair of the commercial humidifiers or "cool-mist vapourizers" at medium setting and the De Vilbiss model 65 ultrasonic nebulizer. The cloud content output from the nebulizer could be varied by varying the amount of electrical power applied to the piezoelectric crystal in the nebulizer. Averaged measured droplet size distributions using the cumbination of cloud generators described above is shown in Fig. 1.3. The cloud sizes were measured by the CSASP particle scattering counter and corrected in accordance with particle response calculations of

Pinnick and Auvermann (1979). The number size distribution spectrum shows a bimodal structure and represents the shape of the droplet size spectrum normally encountered at the later stages of natural cloud development.

1.4. Liquid Water Content of Laboratory Cloud

The prediction of atmospheric extinction from a measureable fog or cloud microphysical parameter such as liquid water content is of considerable practical interest. It is important that absolute methods for the measurement of liquid water content are carefully evaluated. Experimental techniques used to measure absolutely liquid water content of laboratory cloud are described below.

One of the first more reliable methods for the measurement of the liquid water content of fog was used by Houghton and Radford (1938). The amount of fog water was measured by passing a known amount of fog laden air through a series of finely spaced thin wire screens. An impaction method is also used here whereby the cloud droplets impact onto a series of flannel filters. This method was first used by C.W. Bruce (personal communication) and is referred to by Bruce et al. (1980). A schematic diagram of the liquid water impaction device is shown in Figure 1.4. The core of the liquid water content (LWC) device consists of an aluminium ring system which consists of a series (usually 4) circular sheets of flannel material resting on a fine gauge metal perforated screen or gauze. A threaded collar is used to firmly secure the filter material when the cloudy air is drawn through the device. An o-ring assembly is used to ensure that no extraneous air is drawn into the system. A compressor pump (P) together with a calibrated rotameter (R) was used to give the volume of cloudy air drawn through the filter assembly over a selected time period. An electronic timer circuit in conjunction with a solenoid and a relay was used to actuate the aspiration pumps. It also served to remove a flap positioned directly over the intake tube to prevent cloudy air from entering the LWC device before sampling. The timer circuit was used to preselect the sampling period for the experimental measurements. Subsidiary comparative measurements were made of the air flow at the entrance and exit ports of the LWC device due to relatively small pressure drop in the system and appropriate corrections were made to the incoming airflow values as inferred from the rotameter R readings. Measurements using a range of different numbers of flannel filters indicated that 4 flannel filters were sufficient to capture all of the cloud water under typical operating conditions.

A second identical LWC device was placed close to the LWC impactor to serve as a reference. Cloudy air was not aspirated through the reference LWC device, rather the cloud droplets were allowed to fall onto the filter assembly over the same sampling period as the measuring system. It was found that the amount of cloud liquid water collected in the reference filter was significant and must be taken into account in order to take reliable and accurate liquid water content measurements. The filter ring assembly was preweighed on an Oertling balance (typical weight $\sim$30 g) and stored in a dessicator. It was usual to weigh the filter, using the Oertling balance, immediately after the cloud was drawn through the LWC device.

Another arrangement was also set up to measure liquid water content of the cloud directly. This incorporated a top loading Sartorius model 1212 MP balance. A schematic diagram of the system is shown in Fig. 1.5. Cloud laden air is drawn through a funnel shaped impactor which is packed with flannel material, by means of a compressor pump. A rotameter, R, is also in tne line to measure the total volume of cloud sampled. A housing surrounds the impactor which is mounted horizontally, in order to minimise cloud from entering the device under conditions of no suction. The housing has an opening of diameter equal to the impactor tube. Recordings of cloud water content could be made directly with the top balance system. The cloud water content per unit volume was obtained from the mass flow rate measurements of the device.

A comparison was made between the direct filtration methods using the vertical tube arrangement with its reference tube and the top loading balance arrangement with its horizontal filter assembly. Both systems were adjacent to one another in a 1 m^3 chamber lined with water absorbing black material which was pre-wetted to yield a water saturated environment for the cloud droplets. The cloud was produced by a commercially available "cool mist vapouriser" or humidifier whose output was controllable by a range of baffle settings. The results of the LWC comparison are given in Table 1.1.

It can be seen that in general, agreement between the two filtration methods is good. Agreement is somewhat mitigated as the filter material in the top-balance assembly becomes more wetted, resulting in an apparent loss of collected cloud water. It is also clear that the use of a reference impaction assembly is imperative when using the direct filtration technique for the measurement of liquid water content.

1.5. Data Acquisition

Recording of the radiation data was facilitated by means of a digital panel printer (Datel Model DPP-Q7). The Data Acquisition system (PDS-200) was used to record and display size distribution data in histogram form, as measured by the Knollenberg particle scattering counter - model CSASP-100. A Hewlett-Packard Model 5055A digital printer was used to record the particle size channel data which was displayed on the PDS-200 CRT screen.

The PDP8-E minicomputer system was linked successfully to the data acquisition system (PDS-200) of the particle scattering counter. The analogue data from the radiation probe detectors and the electronic top balance was also fed into the PDP8-E minicomputer system. Access to the main frame computer (DEC-20) which contains the main Mie Lorenz scattering computer routines (to be described in Section 2.2) was facilitated by a DEC SPKL8-JA terminal interface for a 9600 baud rate. Because of the occurrence of a number of failures in the PDP8-E mini computer (for example, Memory Bank connector failure), and the serious disruption in the research programme that would result from a major breakdown in the PDP8-E, and the increasing difficulty of obtaining component parts it was decided to opt for a microcomputer based data acquisition system. The microcomputer Data Acquisition System is based on a BBC microcomputer (Model B). Two ports an analogue voltage imput port and an 8-bit wide digital input/ output port are standard features of the microcomputer. A Shugart SA 300 3½" disc drive and an Epson FX-80 line printer are connected to the microcomputer providing permanent storage and hard-copy display of data. The monitor is a "CUB" Microvitec 2 colour monitor which is a medium resolution colour monitor and a high resolution monitor in monochrome. The microcomputer can act as a computer terminal which is connected to a DEC system-20, a mainframe computer system. A special Read Only Memory (ROM) chip called a terminal emulator has been installed. The program written into the ROM was written by the Computer Science Department of Sussex University, England. The microcomputer can emulate, or act like, several types of computer terminals such as the Digital Corporation VT52. The Central Processing Unit or CPU is based on a 6502 microprocessor and operates at a clock frequency of 2 MHz.

The particle data Acquisition system (PDS-200) associated with the particle counter was interfaced to the BBC microcomputer. Data was transmitted from the BBC microcomputer to the DEC system 20 mainframe computer, and was facilitated by means of a softwate program X READ2 on the mainframe computer. A system program called MLAB is used to analyse the data which is stored in the user Directory on disk.

1.6. Experimental Measurement of Middle IR Extinction and Liquid Water Content

The measurements were made in the environmental cloud housing of volume 1 m^3 with the optical arrangement as shown in Fig. 1.1. Details of the apparatus and ancillary equipment used have been already described in the previous sections. The vertically polarised CO_2 laser beam traversed the chamber pathlength and emerged through a small aperture in the exit wall of the chamber. The aperture in the detector probe was reduced down to 3 mm diameter in order to minimize the entry of forward scattered radiation into the detector (Deepak and Box, 1978 a,b).

A homogeneous path is usually assumed when the extinction coefficient σ_e is derived from the Beers-Lambert law of

$$I/I_o = \exp(-\sigma_e L) \tag{1.8}$$

where I_o is the incident radiation intensity and I is the intensity after traversal of path length L through a (cloud) medium. Departures from cloud homogeneity will underestimate the inferred extinction coefficient.

A useful technique for determining the extent of cloud homogeneity has been devised in this laboratory. The apparatus essentially consists of a radiation detector which is mounted inside the cloud housing, with the detector being translated through the cloud on a threaded rod assembly. A He-Ne laser is directed onto the detector which is a UDT FIL-100V silicon photodiode operating in the photovoltaic mode. The detector mounting is driven by a motor control module (whilst the scanning rate of the detector is set by a controlled oscillator frequency, with 5 V amplitude). The direction of rotation of the threaded rod can be reversed by switching a 100 μF capacitor between the motor inputs. The motor and control electronics are fan cooled. Scanning rates of between 30 seconds and 3 minutes are readily achieved whilst mechanical gears are needed to extend this range. A narrow jet of cloud free air is continuously directed across the face of the detector during a scan in order to prevent cloud deposition on the detector itself.

A non-cloud scan ensured a uniform response of the detector along the transmission path. A good representation of cloud homogeneity along the transmission path is shown in Fig. 1.6 for the cloud generators located in their normal symmetrical position in the laboratory chamber, where a 45 degree slope entails 100 per cent homogeneity. Fig. 1.6 shows the degree of inhomogeneity in the cloud over a transmitted path of 0.7 m in terms of optical depth, $\ln(I/I_o)$ plotted against path distance. Most cloud scans with this technique

have yielded results similar to those in Fig. 1.6 indicating a high degree of homogeneity of cloud in the chamber. This is an important finding for our particular cloud chamber in that it obviates the need for several liquid water measurement devices to be placed along the transmission path. It also implies that in general extinction measurements in the chamber do not require correction for inhomogeneity along the transmission path. It should be remarked that checks for inhomogeneity are desirable particularly in chambers of large dimension.

Both broad cloud droplet size distribution using "cool-mist" vapourizers and narrow droplet size distributions using a De Vilbiss model 65 ultrasonic nebulizer were used in a 1 m^3 laboratory chamber. Simultaneous measurement of extinction coefficient σ_e, m^{-1} at the CO_2 laser wavelength λ = 10.591 μm and liquid water content W, gm^{-3} using the direct filtration methods outlined in section 1.4 were made using two distinct experimental procedures: The first procedure involved point measurements of σ_e and W after the cloud had been allowed to reach a steady state condition. Point measurements of σ_e and W are shown in Fig. 1.7. The error bars of the liquid water content parameter indicates the spread in liquid water using the two filtration methods described in 1.4. Isolated points without error bars indicate measurements with the vertical tube filtration method only.

The measured points reveal the ratio σ_e/W being less than the predicted value of 147, shown by the solid line in Figure 1.7 as inferred from Eq. (6) using the analysis of Chylek (1978) and Pinnick et al (1979). The largest deviations from prediction occur for the broader size distributions as produced by the cool mist vapourizers. The value of extinction coefficient σ_e inferred from the relation

$$\sigma_e = 3\pi c.W/2\lambda\rho$$

is overestimated for droplet radius r > 14 μm. Impactor size measurements, which will be described in Section 3 of this report indicate that between 30-35% of the droplet number concentration possess radii in excess of 14 μm, when produced by the cool mist vapourizer generators. Accordingly σ_e/W is overpredicted which is in accordance with the measurements in Fig. 1.7 which are between 10-20 lower than predicted from Eq. (1.9).

The second experimental procedure allowed the cloud to reach steady state conditions and then the cloud generators were switched off in order to make continuous simultaneous measurements of σ_e and W during cloud decay. Narrower size distributions produced from the ultrasonic nebulizer were mainly

used for the decay measurements. Typical experimental results are shown in Fig. 1.8 and Fig. 1.9 for a liquid water content range up to 7 gm^{-3} and for a lower liquid water content range from 2.5gm^{-3} down to low values of LWC. Both figures show good agreement with the prediction of Eq. (1.9) shown by the solid line and they represent the first set of continuous simultaneous measurements of σ_e and W.

Thus the linear relationship as predicted by Chylek (1978) between liquid water content and IR extinction has been experimentally verified down to relatively low values of cloud water content representative of natural cloud values. It is also seen that underestimation of the extinction coefficient occurs for size distributions containing a sizeable proportion ($\sim$30-35%) of drop sizes exceeding about 14 μm radius.

2. EXTINCTION AND BACKSCATTER IN WATER CLOUDS AT VISIBLE WAVELENGTHS

2.1. Introduction

Section 2 describes numerical calculations of extinction and liquid water content of cloud and fog at infrared and visible wavelengths, based on 156 measured cloud droplet size distributions and on measured fog size distributions. Calculations are also presented of extinction and backscatter coefficient at visible and near IR wavelengths. The first definitive simultaneous measurements of both backscatter coefficient and extinction coefficient at visible (He-Ne Laser) wavelengths are described. Since a more complete account of this section is contained within Appendix 1 (Pinnick, Jennings et al, 1983) in some detail and to a lesser extent in Appendix 2 (Jennings, 1983) the more salient features will only be presented in this section.

2.2. Mie-Lorenz Scattering Computer Programmes

Mie-Lorenz scattering computer codes were incorporated successfully onto the University's main frame DEC-20 computer. A DEC VT 50 VDU terminal with direct access to the main frame computer was acquired. In addition the Microvitec colour monitor lined to the BBC microcomputer also served as a terminal to the DEC-20

The Mie scattering algorithm of Davé (1968) used in the Mie-Lorenz scattering code, which uses downward recurrence in the computation of the complex function A_n is numerically stable but time consuming. The criterion for deciding between upward recurrence (is faster) and downward recurrence is presented by Wiscombe (1980) and is incorporated into our Mie scattering algorithms. When downward recurrence has to be used, the recommendation of Wiscombe (1980) was adopted: i.e. downward recurrence was initialized using the Lentz (1976) method rather than Davés (1969) method, requiring significantly fewer number of iterations to calculate A_n (mx).

The computation of scattering amplitudes S_1 and S_2 is achieved using Wiscombe's (1980) algorithm, and is faster than the standard method for particle response and scattering cross-section calculations. The small particle approximation of Wiscombe (1980) was also inserted into the Mie scattering algorithms. Values of efficiency factors using these modified routines give agreement to at least 6 significant figures with values using the original Davé routines.

We now have facility to calculate reliably and accurately:

(i) Volume extinction, absorption, scattering and backscatter coefficients

for log-normal, gamma and power law distributions.

(ii) Efficiency factors (in tabular and plot form) for extinction, absorption, scattering and backscatter.

(iii) Forward scattering corrections for monodispersions of particles for extinction measurements, in terms of the path averaged correction factor R (Deepak and Box, 1978) pertinent to our experimental open detector arrangment.

(iv) Particle response scattering cross-sections for particle light scattering instruments, such as the Knollenberg CSASP-100 particle counter. An example of particle counter response for the CSASP-100 instrument for water droplets and NaCl particles is shown in Figure 2.1.

(v) Volume extinction, absorption, scattering and backscatter coefficients from input of data in histogram format. This is of particular relevance to computations using data from the Knollenberg particle scattering counter.

2.3. Middle IR Extinction and Liquid Water Content in Cloud

It has been shown theoretically and verified numerically (Chýlek, 1978; Pinnick et al, 1979) that an approximate linear relationship of the form of equation (1.6) exists between middle infrared extinction (around λ = 11μm) and liquid water content of fogs. The σ_e - W relation has been verified experimentally for laboratory generated cloud (this work, Section 1), Bruce et al (1980) and Gertler and Steele (1980). Natural cloud droplets of course can be much larger than those in laboratory cloud or fog. For this reason we might not expect relation (1.6) to be applicable to all clouds, particularly if droplets with radius r > 14 μm dominate either extinction or liquid water content. To investigate quantitatively the magnitude of the error involved in the application of (1.6) to clouds we again made Mie calculations of the extinction coefficient and the liquid water content for 156 cloud droplet size distributions summarized in Table 2, Appendix 1. The results of these calculations are compared to the size- distribution-independent prediction (1.6) in Fig. 2.2). (The effect of gaseous absorption is small and has been neglected). Except for cumulonimbus, nimbostratus, cumulus congestus, orographic and some stratus type clouds (which contain significant numbers of large (r > 14 μm) droplets) relation (1.6) is within a factor two of the numerical results. This comparison thus reaffirms the conclusion of Chýlek (1978) that at between 10 and11 μm there exists a nearly-unique relation between extinction coefficient and liquid water content of the form of Eq. (1.6) for nonprecipitating clouds.

2.4. Visible Extinction and Liquid Water Content in Cloud

A high degree of correlation between visible extinction and liquid water content of cloud or fog cannot be expected to hold in general as borne out by the work of Chýlek (1978) and Pinnick et al (1979). Chýlek (1978) has shown that a linear relationship between visible extinction and liquid water content, independent of size distribution will only hold providing the maximum allowable droplet radius does not exceed 0.55 μm - clearly at variance for typical cloud and fog droplet sizes. Indeed visible extinction can vary by approximately an order of magnitude for a particular LWC value as shown by Pinnick et al (1979) and reproduced in Fig. 2.3.

Although Pinnick et al (1978) found maximum radius values for haze particles of about 2 μm, some haze distribution will have a significant proportion of the size distribution less than 0.55 μm. In these circumstances linearity between visible extinction and LWC will be expected. At near infrared wavelengths where the maximum allowable radius increases to 1.2 μm under which conditions extinction is linearly related to LWC, calculations by Pinnick et al (1978) indeed show linearity between σ_e and W at wavelength λ = 1.2μm for the haze size distributions.

It was pointed out recently by Jennings (1983) that it is extremely unlikely that extinction will be linearly related to number concentration for fog (or cloud) size distributions at visible wavelengths.

2.5. Extinction and Backscatter in Water Clouds at Visible Wavelengths

Twomey and Howell (1965) found that there exists a relation (though not a unique one) of the form σ_e = constant σ_b, between backscatter σ_b and extinction coefficient σ_e using Gaussian and Poisson size distributions. Curcio and Knestrick (1958) made simultaneous measuremtns of backscatter and extinction in cloud and found a proportionality between extinction and backscatter coefficients of the form $\sigma_e = \sigma_b 1.5$ for weather conditions including fog, fog and drizzle and clear weather. However, there is considerable leeway in determining the exponent in this proportionality from their measured data (their figure 4). In addition the effects of fog inhomogeneities and multiple scatter contributions to the backscatter and transmission signals probably caused uncertainty in their data. Carrier et al (1967) calculated extinction and backscatter coefficients for eight model cloud drop spectra at visible and middle IR wavelengths. At 0.694 μm wavelength,

they obtain an average value for all 8 cloud models of 1/22.6 for the backscatter to extinction ratio. More recently, Derr (1980) predicts a value of 1/16.76 for the backscatter to extinction ratio at $\lambda = 0.694$ μm for a set of Deirmendjian cloud size distributions appropriate to cumulus, continental cumulus and cumulonimbus clouds.

The backscatter coefficient σ_b of a polydispersion of spherical cloud droplets described by a size distribution $n(r)$ and refractive index m is given by

$$\sigma_b = \frac{1}{4\pi}\int \pi r^2 \, G(m,x) \, n(r) \, dr \qquad (2.1)$$

where $G(m,x)$ is the backscatter gain defined as 4π times the ratio of the backscatter differential cross section to the geometric area.

Cloud is dominated by droplet sizes with radii $2\ \mu m < r < 85\ \mu m$ corresponding to size parameter $12 < x < 500$ at a wavelength $\lambda = 1.06\mu m$. If we can assume that atmospheric cloud droplets generally have slowly varying concentrations over radius intervals of the order $\Delta r \approx 1.6$ μm at near IR wavelengths (1.06μ) then the Mie efficiency factor for extinction Qe can be approximated (see Appendix 1 for further details) by

$$Q_e = 2\,(1 + x^{-2/3}) \qquad (2.2)$$

The backscatter gain $G(m,x)$ can also be approximated by

$$G = g(\lambda)\,(1 + \delta x^2) \qquad (2.3)$$

where $g(\lambda)$ is a slowly varying function of wavelength and $\delta << 1$.

The use of approximations (2.2) and (2.3) in equations (1.1) and (2.1) leads to the cloud extinction coefficient σ_e being related to the backscatter coefficient (Pinnick et al, 1983 shown in Appendix 1) and has the form

$$\frac{\sigma_e}{\sigma_b} = \frac{8\pi}{g}\left[1 + k^{-2/3}\cdot\frac{\langle r^{4/3}\rangle}{\langle r^2\rangle} - \delta\left\{k^2\frac{\langle r^4\rangle}{\langle r^2\rangle} + k^{4/3}\frac{\langle r^{4/3}\rangle\langle r^4\rangle}{\langle r^2\rangle\langle r^2\rangle}\right\} + O(\delta^2)\right] \qquad (2.4)$$

where k : the wavenumber and $\langle r^n \rangle$ is the nth moment of the droplet size distribution. If one takes account of the higher order terms in the above equation, using cloud gamma size distribution models of Diermendjian (1969), then these higher order terms are typically 10% of the leading term for non-precipitating clouds. If errors of this order are acceptable then Eq. (2.4) reduces to the simple form

$$\sigma_e = \frac{8\pi}{g}\,\sigma_b \qquad (2.5)$$

where the extinction is a linear function of backscatter, independent of drop size.

To test the range of validity of the linear extinction-backscatter relation (2.5) for cloud we calculated using Mie theory and indexes of refraction of water given by Hale and Querry (1973) the extinction coefficient according to Eq.(1.1) and the backscatter coefficient according to Eq. (2.1) for 156 cloud droplet size distributions measured in the major cloud types. The sources of these measurements together with the range of droplet sizes measured and other pertinent information is listed in Table 2, Appendix 1. The main sampling technique employed to obtain the cloud droplet size distributions was that of impaction of droplets onto coated slides or replicators whose collection efficiencies were known. The practical lower limit for detection of cloud droplets by the impaction technique is around 1.5 μm radius. The sole cloud size determination by a light scattering counter (Ryan, et al, 1972) was calibrated by means of uniformly seized water droplets. Only non-precipitating clouds were used in the analysis and measurements which showed evidence of glaciation were excluded.

The numerical calculations of extinction and backscatter are shown compared to our linear relation (2.5) in Fig. 2.4 for λ = 1.0μm. {As an aside we note that Derr's (1980) relation between extinction and backscatter $\sigma_e = 18.0\ \sigma_b$ is negligibly different from our relation (2.5) at this wavelength.} For all considered cloud size distributions the relation (2.5) is within 50% of the numerical results. Thus the numerical results suggest that cloud extinction coefficients can be inferred from measurement of the backscatter coefficients directly from Eq. (2.5), without need to know details of the cloud droplet size distribution. If knowledge of the droplet size distribution is available, then extinction coefficients could be determined more accurately by employing the better approximation (2.4).

The simple linear extinction-backscatter relation (2.5) should be particularly useful for lidar probing of cloud edges, where entrainment causes intense evaporation and severe distortion of the droplet spectra, and where as a result the spectra may not be representative of the entire cloud. The associated wide spatial and temporal variability in the droplet spectra will not prohibit the use of our relation (2.5) to infer extinction coefficients from lidar backscatter coefficients, since the relation is size-distribution-independent.

Of course cloud backscatter coefficients can be determined from lidar return signals (in a straight-forward way) only in the absence or neglect of multiple scattering contributions to the lidar signal. It follows that application of (2.5) to obtain cloud extinction coefficients from lidar returns might be restricted to the edges of clouds where the contribution of multiply-scattered

photons is small.

2.6. Experimental Verification of the Extinction-Backscatter Relation at Visible Wavelengths.

The apparatus used to measure the extinction and backscatter coefficients is shown schematically in Fig. (2.5). In an attempt to determine experimentally the accuracy of the extinction-backscatter relation (2.5) we decided to restrict our study to laboratory simulations of cloud (because of the difficulty in making atmospheric measurements). We generated in a cubical 1.0 m^3 chamber polydispersions of cloud droplets using "cool-mist" vaporizers and a De Vilbiss model 65 ultrasonic nebulizer described in section 1.3. Chamber saturation and cloud stability was maintained by soaking a black matt cloth lining the chamber floor with water. The matt cloth also served to reduce stray light levels. Droplet distributions obtained with these generation schemes were generally unimodal with a range of drop sizes characteristic of clouds. Interestingly, the nebulizer distributions were narrower than those for the cool-mist vaporizers, but they resulted in higher backscatter and extinction levels because of their much higher number concentrations.

Backscatter and extinction measurements were made simultaneously on the laboratory simulated clouds employing a 5.4 mw He-Ne laser source, a synchronous radiometer (Laser Precision Corporation model Rk 5100) for monitoring laser power, a pyroelectric detector (LPC model RkP-545), for measuring transmitted laser power, and a silicon photodetector (United Detector Technology model FIL-100V) for measuring backscattered light. Measurement of the backscattered light was facilitated with a highly reflective (>99.3%) circular mirror judiciously positioned on the axis of the laser beam so that a small (3.16 mm) hole drilled through its center would admit the laser beam into the fog chamber, and at the same time intercept light scattered in the near-backward direction. The mirror was tilted about 9^o (from the laser beam direction) to reflect the backscattered radiation onto the photodetector. The silicon photodiode has a responsivity of 0.40 A $Watt^{-1}$ at λ = 0.6328 μm. The backscatter signal was then amplified and monitored by an accurate digital voltmeter measureable to microvolts. Test measurements of laser radiation were in agreement to within 1% using the photodiode detector and the pyroelectric detector probe. Precautions were taken to ensure that detector aperatures were small enough that forward scattering corrections to both transmission and backscatter signals (Deepak and Box, 1978) could be neglected.

The extinction coefficient σ_e (km^{-1}) is determined from the Lambert-Bouguer Law (Eq.1.8) which assumes homogeneity along the cloud path. I_o is the measured radiation signal in the absence of cloud, I is the measured signal in the presence of cloud. The backscatter coefficient σ_b (km^{-1} sr^{-1}) is derived from the expression

$$I_B = \int_b^{b+L} I_s \sigma_b \frac{A}{(b+\ell)^2} e^{-2\sigma_e \ell} d\ell \qquad (2.6)$$

where I_B is the measured backscatter signal (in Watts).

I_s: absolute value of the He-Ne laser radiation (in Watts).

σ_b: the backscatter coefficient (km^{-1} sr^{-1})

A : photodetector area

b : path length between the photodetector and the chamber entrance, equal to AB+BC (see figure 2.5)

The effective photodetector area was reduced by 8% due to the 3.16 mm diameter hole in the reflecting mirror.

Simultaneous measurements of extinction and backscatter coefficients were recorded every ten seconds for each experimental run. The half angle θ subtended by the open pyroelectric detector is not more than 0.1^o and so forward scattering corrections to extinction measurements for the droplet media are less than a few percent in accordance with the calculations of Deepak and Box (1978 a,b). Measurements of radiation using a range of entrance apertures to the photodiode detector indicated that multiply scattered radiation did not contribute to the extinction signal. The silicon photodetector output was offset to a minimum signal level in the absence of cloud. Signal to noise ratios > 200 prevailed for the backscatter measurement.

Simultaneous measured values of extinction and backscatter coefficient made at 10 second intervals are presented in Figure 2.6, for different experimental runs. The majority of measurements are for the broader size distributions produced by the pair of humidifiers, the narrow size distributions generally produced the largest extinction and backscatter values (data indicated by □ in Figure 2.6). The ratio of extinction to backscatter coefficients at the He-Ne wavelength λ = 0.6328 μm is within 20% of the predicted relation of $\sigma_e = \frac{8}{g(\lambda)} \sigma_b$ where the equation is a linear function of backscatter, independent of droplet size, for clouds with liquid water contents ranging from 0.05 up to 1 gm^{-3}. Agreement between experiment and theory is best for polydispersions of droplets having a broad range of sizes (these correspond to data points in Fig. 2.6 where $\sigma < 30 km^{-1} sr^{-1}$). The reason for this can be understood

by examining the more exact backscatter-extinction relation (2.4). For broad distributions the higher order terms in (2.4) tend to cancel since they are of opposite sign and of comparable magnitudes, making the zero order approximation (2.5) a good one. For clouds (generated with the nebulizer technique) having a narrow distribution of smaller droplets (corresponding to data points where $\sigma_b > 30\ km^{-1}sr^{-1}$) the agreement between experiment and theory is not quite as good. For these distributions the second term in the extinction-backscatter relation (2.4) is no longer concelled by the (negative) contribution of the term of order δ, rendering the linear (zero order) relation (2.5) less accurate.

The above measurements were made solely for the clouds in a steady-state condition. Measurements were also recorded here for

(a) during the initial build up of cloud,

(b) steady-state cloud conditions

(c) the initial decay interval of the cloud. The cloud size distributions are generated by a combination of two humidifiers at medium setting and the nebulizer whose size distribution is of the form shown in Fig. 1.3. Simultaneous measurements of extinction and backscatter coefficients, recorded at 10 second intervals are presented in Figures 2.7 and 2.8 for both the cloud buildup stage indicated by "O" and the cloud decay stage "●" when the cloud generators were switched off. In general, the measurements agree fairly closely (within about 15%) with the predicted size distribution independent relation - Eq. (2.5).

These experimental measurements - the first such work that is definitive - verifies the linearity of the relation

$$\sigma_e = \frac{8\pi}{9}\sigma_b$$

between extinction coefficient σ_e and backscatter extinction σ_b at visible wavelengths ($\lambda = 0.6328\ \mu m$) for laboratory generated fog/cloud droplet distributions. This result suggests that visible or near-infrared extinction coefficients in cloud of unknown type could be inferred from lidar backscatter measurements alone, without knowledge of the cloud droplet size spectra, excluding complications thay may arise from multiple scattering contributions to the lidar return signal.

3. EXTINCTION AND BACKSCATTER OF WATER CLOUDS AT CO_2 LASER WAVELENGTHS.

3.1. Introduction

Although CO_2 laser technology, which incorporates CO_2 lidar work, is now developing rapidly, efforts to extract attenuation from a CO_2 lidar return have to date been largely statistical in nature. A knowledge of the relationship between backscatter and attenuation would allow the determination of attenuation and backscatter from the return signal of a lidar system using the analytical inversion solution of Klett (1981). However, very little work has been done to date on relating backscatter to extinction at CO_2 laser wavelengths. Some of the principal recommendations which resulted from the workshop on global large aerosols, compiled by Freeman F. Hall, (1983) Chief of the Doppler Lidar program at NOAA, included the necessity of CO_2 backscatter and extinction measurements - both requiring experimental and theoretical work.

We should not necessarily expect the extinction-backscatter relation (2.5) for cloud to be applicable at all wavelengths, since the backscatter gain cannot generally be well approximated by slowly varying functions of size parameter at all wavelengths. To prove this conjecture, the extinction and backscatter coefficients for the previously mentioned 156 cloud size distributions were calculated at several laser wavelengths. An example of the results at the CO_2 laser wavelength λ = 10.6 μm (Fig. 7 Appendix 1) show that for a particular backscatter coefficient the extinction varies by an order of magnitude for different size distributions of droplets.

Despite the scatter in the calculated points of σ_b of Fig. 7 (Appendix 1), a closer examination of the results reveal that the broader drop size distributions within the 156 cloud size distributions investigated shows that the extinction to backscatter ratio attains relatively constant values.

The normalized backscatter cross-section (efficiency factor) Q_{BKS} (m ,x) for water is plotted in Fig. 3.1 as a function of size parameter x using an updated Mie-Lorenz scattering computer code using Wiscombe's (1980) algorithm, details of which are described more fully in Section 2.2. It is seen that the normalized backscatter cross-section oscillates about a constant value for $x > 6$ (radius $r > 10$ μm at λ = 10.591 μm). In view of the fact that calculations show that the extinction cross-section is constant for increasing x for $x > 8$ at λ = 10.591 μm, we can predict that extinction/backscatter will be largely independent of x also for $x > 6$-8.

Calculations indeed show that the extinction to backscatter ratio σ_e/σ_b at $\lambda = 10.591$ μm (P20 CO_2 laser wavelength line) oscillates about a constant value for water droplet radius > 8.5 μm as shown in Fig. 3.2. We predict that broad cloud drop size distributions will give rise to relatively constant values of extinction to backscatter ratios at CO_2 laser wavelengths.

For size parameter $x < 8$ the efficiency factor for extinction Q_e can be approximated by the linear relation (1.4), $Q_e\ (m,x) = c(\lambda).x$ at CO_2 laser wavelengths. The backscatter gain $G(m,x)$ is a rapidly varying function of x (see Fig. 3.1) over the same size parameter range. It follows that for $x < 8$ (droplet radius < 14 μm) at CO_2 laser wavelengths, the extinction to backscatter ratio is a sensitive function of drop size as is borne out by the numerical calculations of extinction and backscatter for natural cloud, shown in Fig. 7 (Appendix 1).

3.2. Experimental Measurement of Backscatter Coefficient and Extinction Coefficient at CO_2 Laser Wavelengths.

(a) Experimental Apparatus and Techniques

Backscatter and extinction measurements were made on laboratory simulated clouds employing the model 941S CO_2 laser source, a synchronous radiometer (model Rk5100) for monitoring laser power, a pyroelectric detector (LPC model RkP-545) for measuring the transmitted laser power and an Infrared Associates Inc. Mercury Cadmium Telluride HgCdTe liquid nitrogen cooled 8-13μm radiation photoconductive detector (Model No. HCT-90) for measuring the backscattered light. Attempt were made to use a similar technique described in Section 2.6 for visible wavelengths whereby a central hole drilled through a metalized mirror surface would admit the laser beam through the cloud chamber and at the same time intercept the backscattered radiation onto the HgCdTe detector. However it was not possible to use this technique because of the occurrence of directly reflected radiation from the internal walls of the hole onto the sensitive detector. The detector was placed close to the CO_2 laser axis in the backward direction, at a distance not more than 5.9 cm from the axial direction, thus subtending an angle not less than 177.4^{o} with the forward direction at the chamber centre. The HgCdTe detector was mounted on an x-y translation stage with vertical height adjustment.

The evaluated detector possessed a metal dewar assembly which contained the necessary liquid nitrogen for cooling the detector. The HCT-90 detector had a sensing area of 1 mm squared. The signal from the detector was fed into a PPA-15-1 pre-amplifier, then into the input of a EG&G Brookdeal Model 9501 lock-in amplifier. A EG&G Brookdeal model 9479 light chopper, operating normally at 1000 Hz served as reference to the lock-in amplifier. The amplifier output from the lock-in amplifier was recorded on a Philips model PM8100 chart recorder. Precautions were taken to reduce stray reflected IR laser radiation from entering the detector during experimental runs. The detector aperture on the pyroelectric probe RkP-545 was maintained at 3 mm to minimise forward scattering corrections to the transmission signal (Deepak and Box, 1978).

The water clouds were produced using "cool-mist" vapourisers on their own and in combination with a De Vilbiss model 65 ultrasonic nebulizer (see section 1.3). Typical droplet size spectra obtained using a two-stage impactor (Garland, 1971) mounted in a wind tunnel are shown in Fig. 3.3, using the "cool-mist" humidifiers at medium (upper figure) and high settings.

particle scattering counter) to be measured. The droplets which impacted onto gelatine slides were viewed and measured microscopically with the aid of a Porton graticule.

(b) Measurement of Backscatter Coefficient and Extinction Coefficient at CO_2 Laser Wavelengths.

Due to the necessarily high sensitivity of the HgCdTe detector, it was not possible to make simultaneous measurement of extinction and backscatter in the chamber cloud. (This is because the backscattered or reflected signal from the walls of the pyroelectric detector probe at the exit end of the chamber greatly exceeded the true signal). The experimental procedure involved firstly the measurement of the initial CO_2 laser intensity (I_o) before entering the chamber followed by measurement of the backscatter signal,interspersed with extinction measurements. Both backscatter and extinction measurements were made for steady-state cloud conditions and during cloud decay. The backscatter coefficient σ_b (km^{-1} Sr^{-1}) is derived from equation (2.6). The absolute value of the CO_2 laser radiation, in Watts, was determined from the pyroelectric RkP-545 probe which was calibrated by means of an Electro Optical Industries Inc. Blackbody Source, model WS 153, of one inch conical cavity with temperature controller providing a temperature range from 50 to 1000°C.

The measured backscatter signal with output from the lock-in amplifier was calibrated by directing a known low CO_2 laser radiation signal onto the HgCdTe detector. The low level CO_2 laser radiation signals were monitored on the model Rk 5100 radiometer operating in synchronization with a CTX-32 external chopper.

Signal to noise ratios of at least > 10 (and generally much in excess of 10) prevailed for the backscatter measurements. Measurements of backscatter coefficient and extinction coefficient at λ = 10.591 μm (unless otherwise stated) are presented in Fig. 3.4. Cool-mist vapourizers were used here to produce the laboratory cloud. Measured values taken in steady state cloud conditions, are indicated by the points "⊖" in Fig. 3.4. The experimental points "●" represent measurements of backscatter and extinction coefficients made during the growth stage of the cloud up to the steady state value.

Most measured values of the extinction to backscatter ratio σ_e/σ_b are above the lower bound line representing a value of 350 in Fig. 3.4. This lower bound value also represents the minimum values obtained for σ_e/σ_b using numerical

calculations of backscatter and extinction coefficient based on 156 measu droplet size distributions (see Fig. 7, Appendix 1). The vast majority of measurements for the cool-mist humidifier cloud yield values of extinction to backscatter ratio from 350 up to 550, as shown in Fig. 3.4. These ratio values reflect the fact that the cloud droplet size parameters were predominantly < than about 6 (radius < about 10 micrometres), a region where the backscatter cross-section possesses much greater values than average (Fig. 3.1).

Fig. (3.2) predicts that the extinction to backscatter ratio is a sensitive function of drop size for droplet radius < 10 μm. This prediction is borne out by the upper measurements in Fig. 3.4 which were performed on a different type of cloud : produced by a combination of the ultrasonic nebulizer with two humidifiers. The narrower size distributions produced the larges backscatter and extinction signals because of their much higher concentrations. It is clear that the measured extinction to backscatter ratio is sensitive to the cloud size distribution over the range of droplet size used.

Measurements were generally made at the CO_2 laser P20 line (λ = 10.591 μm). However some measurements were made at the R 18 line (λ = 10.261 μm) for cloud produced by the combination of nebulizer and two humidifiers. These are shown in Fig. (3.4) and are indicated by "X". They yield larger σ_e/σ_b ratio values, principally because the extinction per unit mass is greater at λ = 10.261 μm than at λ= 10.591 μm (see Pinnick et al, 1979 for details).

3.3. Conclusions

The measurements described in this section represent the first definitive measurements of backscatter and extinction coefficient in laboratory cloud at CO_2 laser wavelengths. The measurements are in reasonably good agreement with numerical predictions on cloud possessing narrow type size distributions as are used here.

The measurements yield relatively constant values for extinction to backscatter ratio for the same common form of size distribution. The ratio values vary between 350 and 550 in these experiments. It is also clear that the measurements show sensitivity of σ_e/σ_b to size distribution when a different shaped size distribution is used.

It is now planned to carry out measurements for broader size distributions where it it predicted (see Fig. 3.2) that the extinction to backscatter ratio becomes fairly insensitive to droplet size.

REFERENCES

Barteneva, O.D. and E.A. Polyakova, 1965: A study of attenuation and scattering of light in a natural fog due to its microphysical properties. Izv. Atmos. Oceanic Phys., 1, 193-207.

Bruce, D., C.W. Bruce, Y.P. Yee, L. Cahenzli and H. Burket, 1980: Experimentally determined relationship between extinction and liquid water content. Applied Optics, 19, 3355-3360.

Chýlek, Petr, 1978: Extinction and liquid water content of fogs and clouds. J. Atmos. Sci., 35, 296-300.

Curcio, J.A. and G.L. Knestrick, 1958: Correlation of atmospheric transmission and backscattering. J. Opt. Soc. Am., 48, 686-689.

Davé, J.V., 1968: Subroutines for computing the parameters of the electromagnetic radiation scattering by a sphere. IBM Rept. 320-3237, IBM Scientific Centre, Palo Alto, Calif.

Davé, J.V., 1969: IBM J. Res. Dev. 13, 302.

Deepak, Adarsh and M.A. Box, 1978a: Forward scattering corrections for optical extinction measurements in aerosol media. 1: Monodispersions. Appled Optics, 17, 2900-2908.

Deepak, Adarsh and M.A. Box, 1978b: Forwardscattering corrections for optical extinction measurements in aerosol media. 2 : Polydispersions. Applied Optics, 17, 3169-3176.

Diermendjian, D., 1969: Electromagnetic scattering on spherical polydispersions, American Elsevier, New York.

Derr, V.E., 1980: Estimation of the extinction coefficient of clouds from multiwavelength lidar backscatter measurements. Applied Optics, 19, 2310-2314.

Eldridge, R.G., 1966: Haze and fog aerosol distributions. J. Atmos., 23, 605-613.

Eldridge, R.G., 1971: The relationship between visibility and liquid water content in fog. J. Atmos. Sci., 28, 1183-1186.

Garland, J.A., 1971: Some fog droplet size distributions obtained by an impaction method. Quart. J. Roy. Meteor. Soc., 97, 483-494

Garland, J.A., J.R. Branson and L.C. Cox, 1973: A study of the contribution of pollution to visibility in a radiation fog. Atmos. Environ., 7, 1079-1092.

Gertler, A.W., and R.L. Steele, 1980: Experimental verification of the linear relationship between IR extinction and liquid water content of clouds. J. Appl. Meteorol., 19, 1314-1317.

Hale, G.M. and M.R. Querry, 1973: Optical constants of water in the 200 nm to 20μm wavelength region. Applied Optics 12, 555-563.

Hall, F.F., Jr., 1983: Atmospheric infrared backscatter: Summary of present knowledge and recommendations for future work. NOAA Technical Memorandum ERL WPL-110, Wave Propagation Laboratory, Boulder, Co.

Houghton, H.G. and W.H. Radford, 1938: On the measurement of drop size and liquid water content in fogs and clouds. Phys. Ocean and Meteor., 6, 1-31.

Jennings, S.G., 1983: Extinction and liquid water content of fog at visible wavelengths. Applied Optics, 22, 2514-2515.

Klett, James D., 1981: Stable analytical inversion solution for processing lidar returns. Applied Optics, 20, 211-220.

Kumai, Motoi, 1973: Artic fog droplet size distribution and its effect on light attenuation. J. Atmos. Sci., 30, 635-643.

Kunkel, B.A., 1971: Fog drop-size distributions measured with a laser hologram camera. J. Appl. Meteor., 10, 482-486.

Lentz, W.J., 1976: Generating bessel functions in Mie scattering calculations using continued fractions. Applied Optics, 15, 669-671.

Pinnick, R.G., D.L. Hoihjelle, G. Fernandez, E.B. Stenmark, J.D. Lindberg, S.G. Jennings and G.B. Hoidale, 1978: Vertical structure in atmospheric fog and haze and its effect on IR and visible extinction. J. Atmos. Sci., 35, 2020-2032.

Pinnick, R.G., S.G. Jennings, Petr Chylek, and H.J. Auvermann, 1979: Verification of a linear relation between IR extinction, absorption and liquid water content of fogs. J. Atmos. Sci., 36, 1577-1586.

Pinnick, R.G. and H.J. Auvermann, 1979: Response characteristics of Knollemberg light-scattering aerosol counters. J. Aerosol. Sci., 10, 55-74.

Pinnick, R.G., S.G. Jennings, Petr Chylek, C. Ham, and W.T. Grandy, Jr., 1983: Backscatter and extinction in water clouds, J. Geophys. 88, 6878-6796.

Roach, W.T., R. Brown, S.J. Caughey, J.A. Garland and C.J. Readings, 1976: The physics of radiation fog: I - A field study. Quart. J. Roy. Meteor. Soc., 102, 313-333.

Ryan, R.T., H.H. Blau, P.C. von Thuna and M.L. Cohen, 1972: Cloud microstructure as determined by an optical cloud particle spectrometer. J. Appl. Meteorol., 11, 149-156.

Twomey, S. and H.B. Howell, 1965: The relative merit of white and monochromatic light for the determination of visibility by backscattering measurements. Applied Optics, 4, 501-506.

Wiscombe, W.J., 1980: Improved Mie scattering algorithms. Applied Optics, 19, 1505-1509.

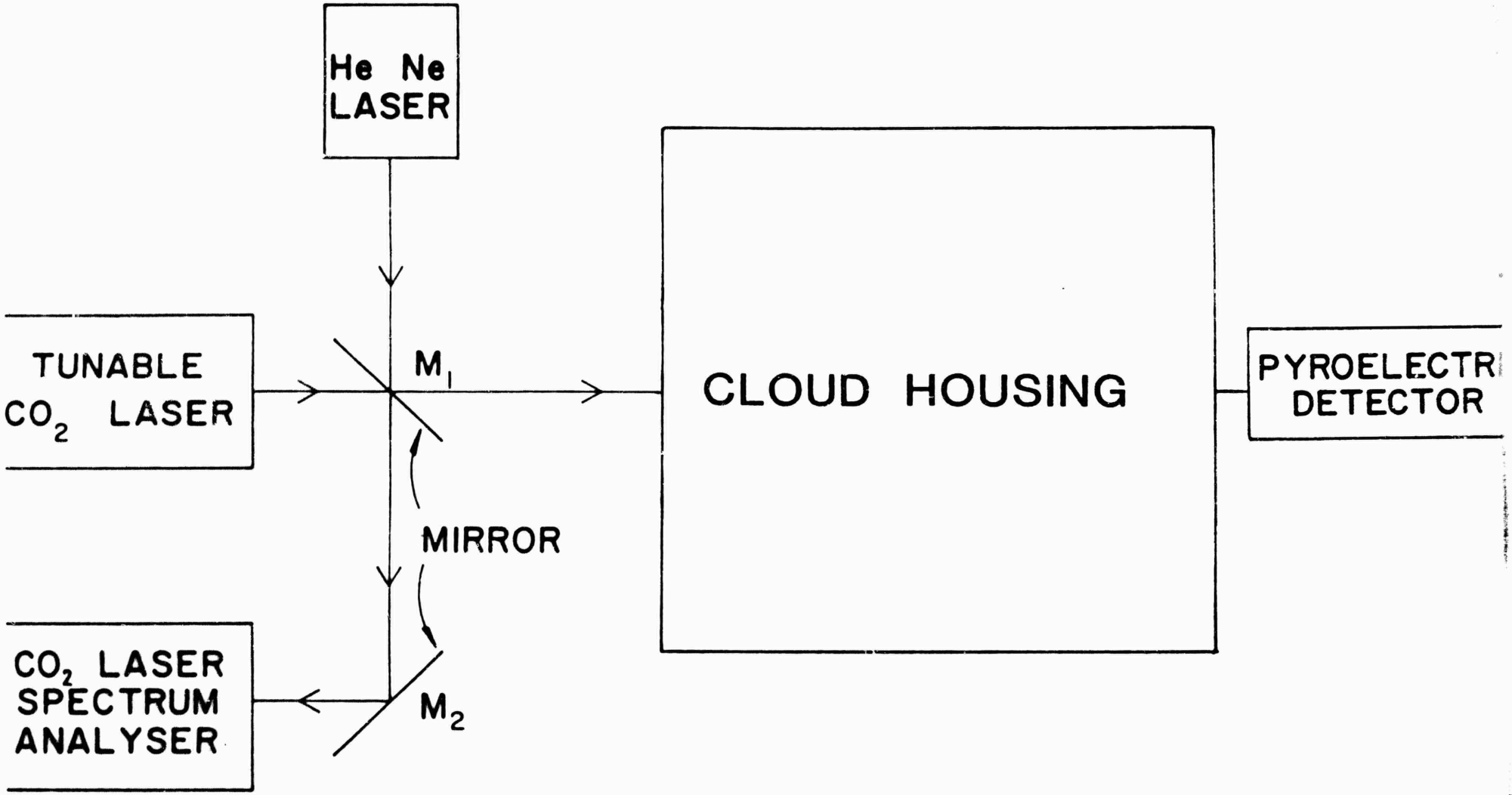

Fig. 1.1. Schematic diagram of optical arrangement used for the extinction coefficient measurements.

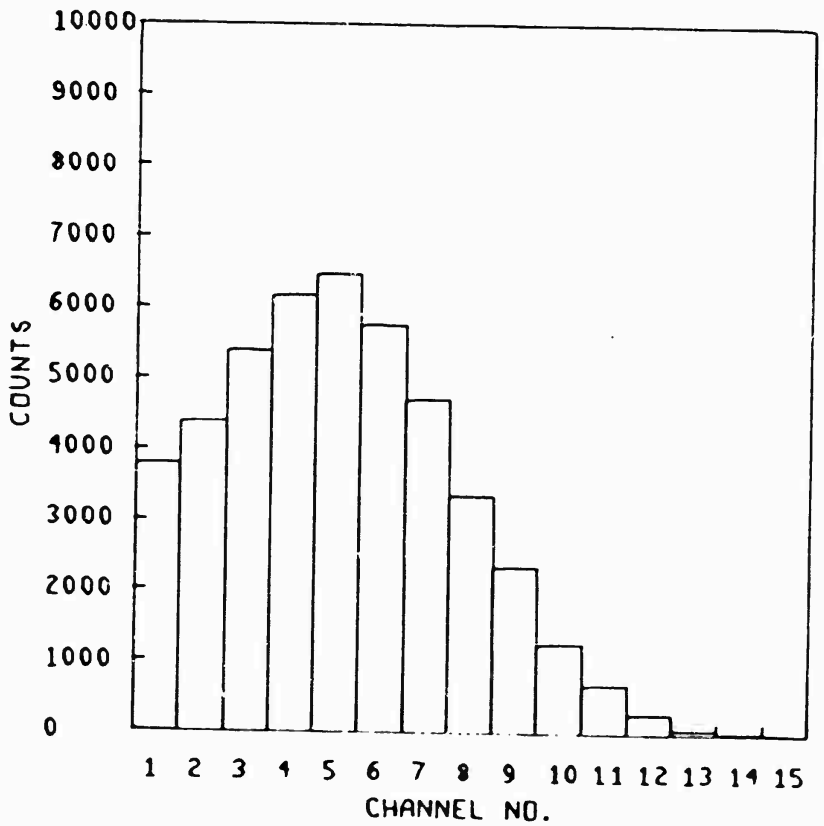

Fig. 1.2. A size distribution histogram from the cloud nebulizer generator.

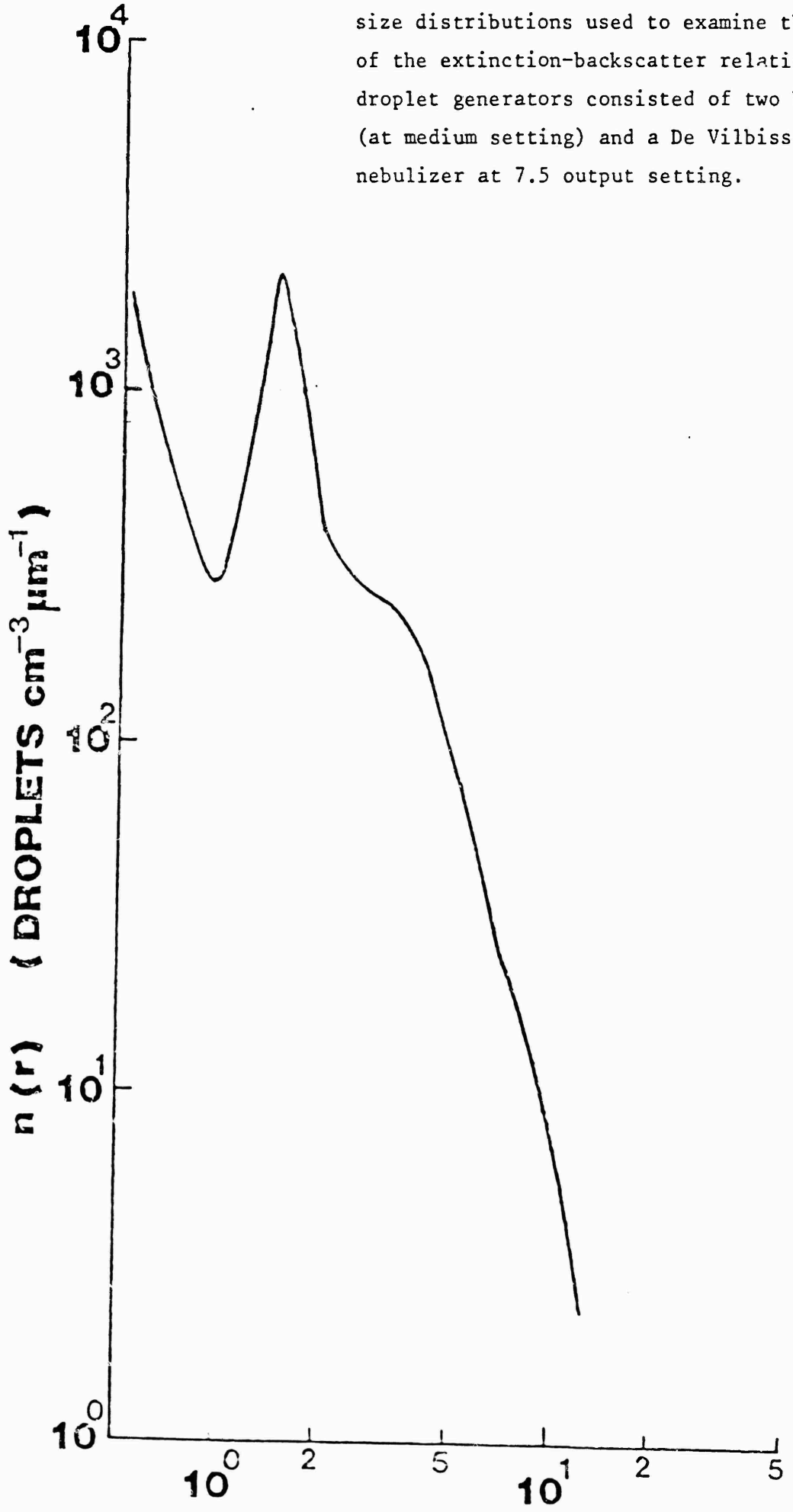

Fig. 1.3 Measured laboratory-generated cloud droplet size distributions used to examine the accuracy of the extinction-backscatter relation. The droplet generators consisted of two humidifiers (at medium setting) and a De Vilbiss Model 65 nebulizer at 7.5 output setting.

Fig. 1.4 LWC MEASUREMENT SYSTEM - DIRECT FILTRATION

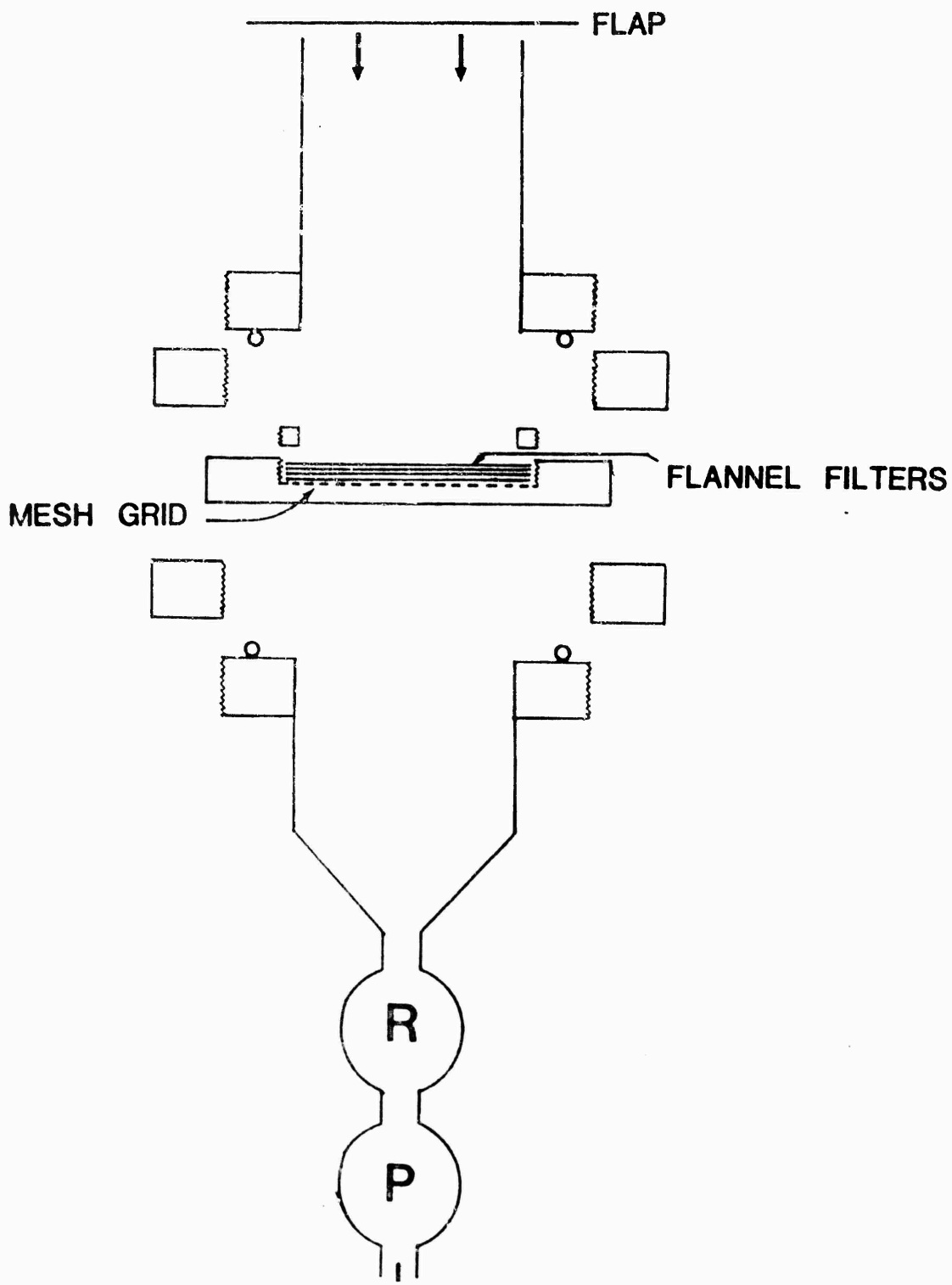

Fig.1.6. Optical depth as a function of transmission path length in the laboratory cloud chamber.

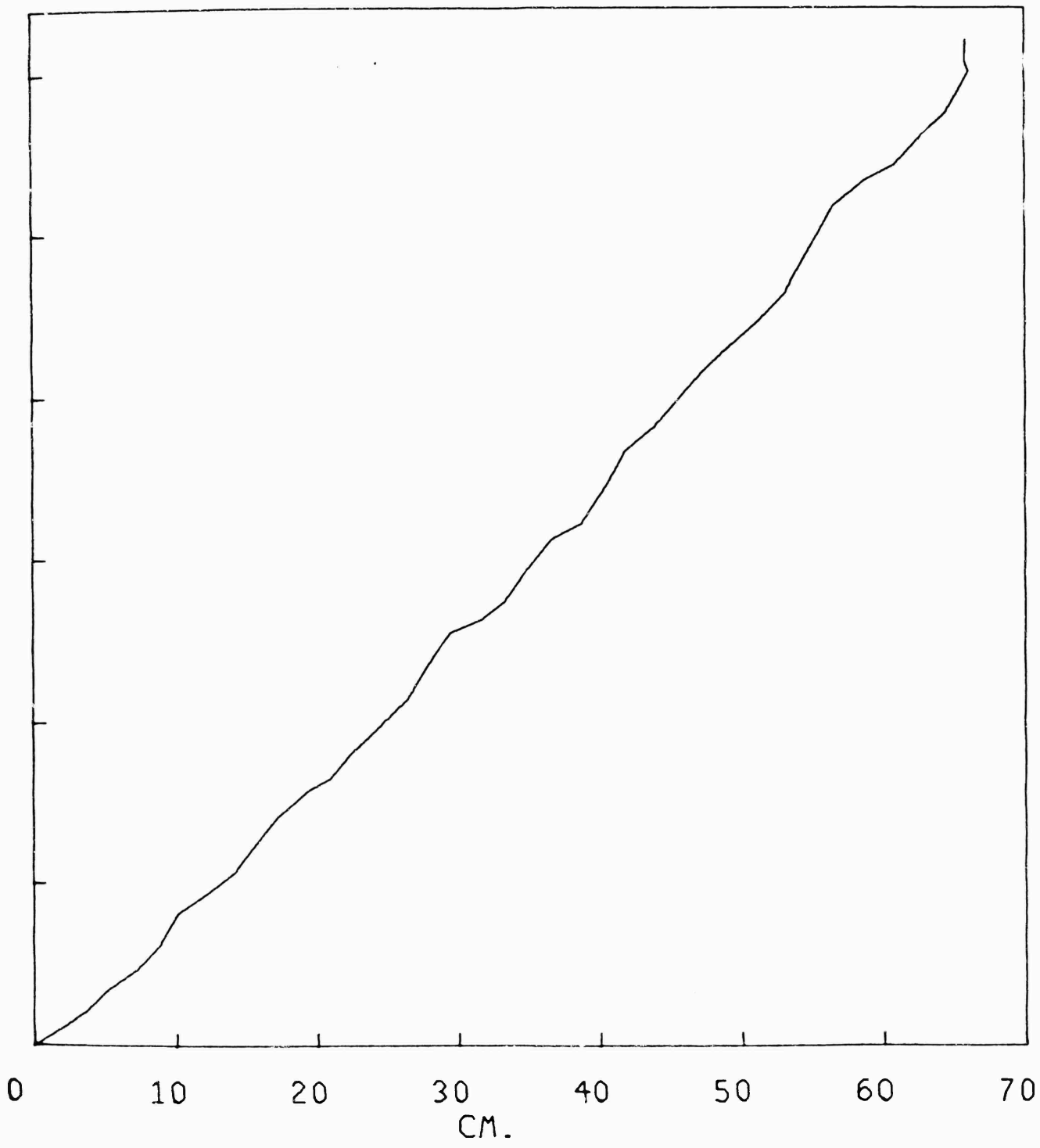

Fig.1.7. Measured values of extinction coefficient σ_e (m^{-1}) and of liquid water content W (gm^{-3}) for laboratory cloud at wavelength λ = 10.591 μm.

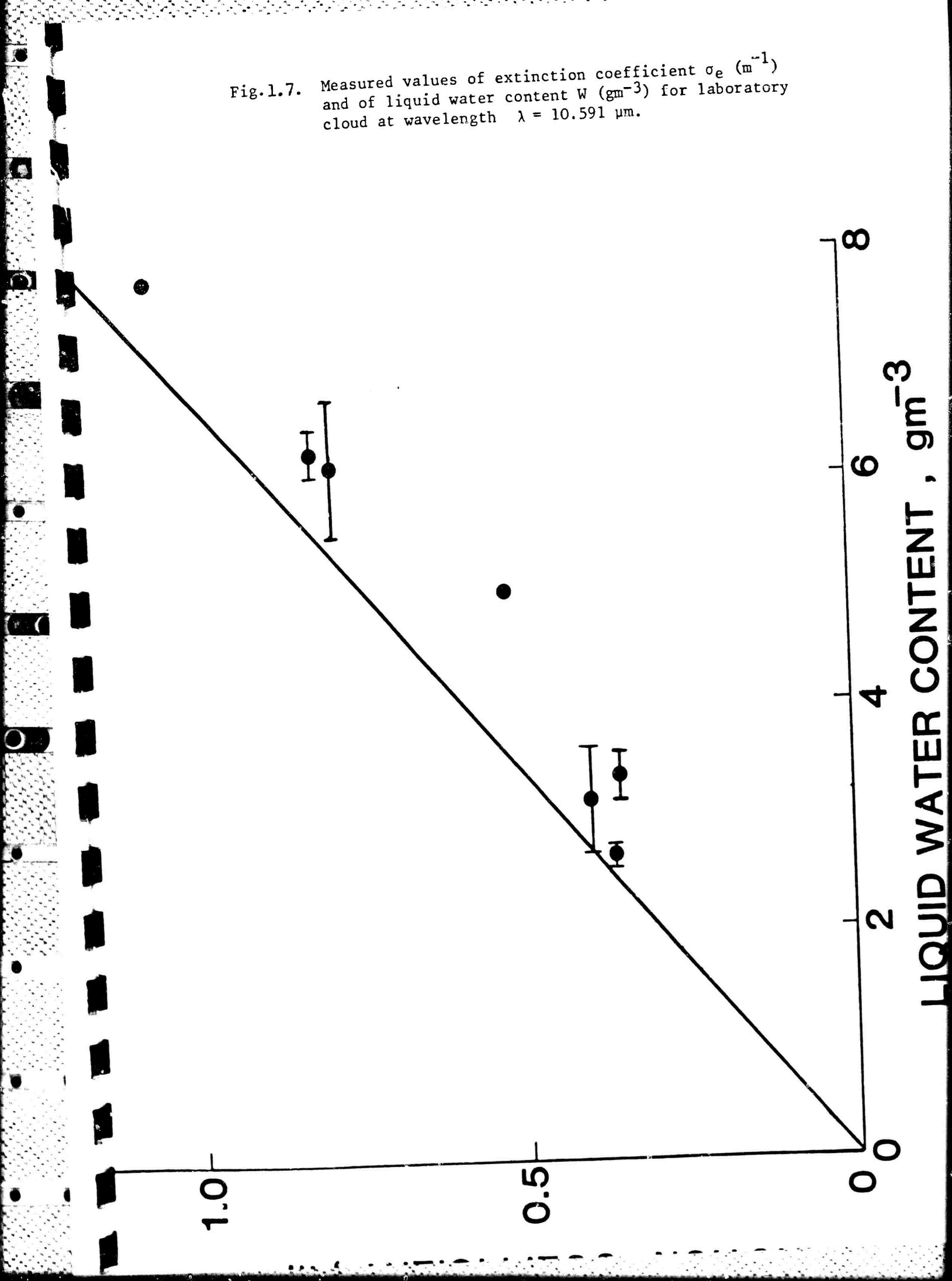

Fig. 1.8 Continuous simultaneous measurements of σ_e and W for laboratory cloud at λ = 10.591 μm. The lower solid line is a best fit to the data. The upper straight line is that predicted by the Chýlek relation.

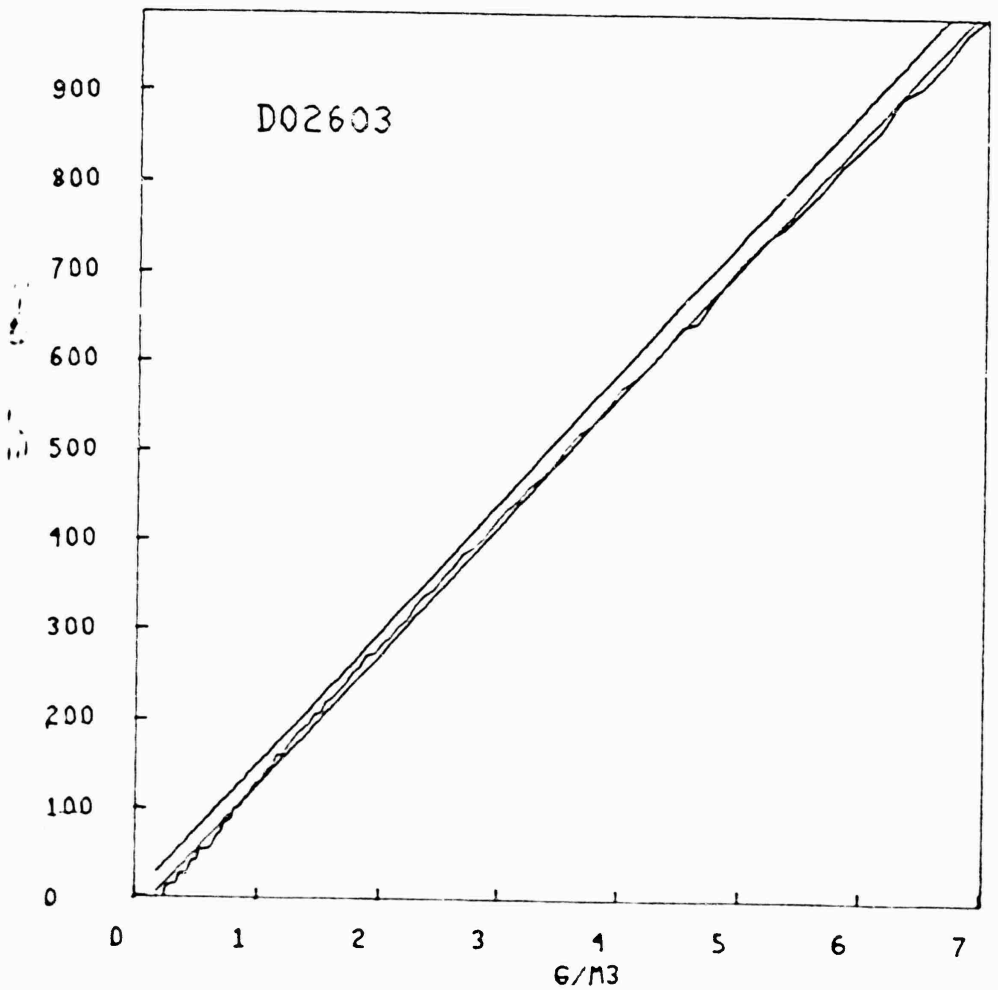

Fig. 1.9 Continuous simultaneous measurements of σ_e and W for laboratory cloud at λ = 10.591 μm. The solid straight line is that predicted by the Chýlek relation.

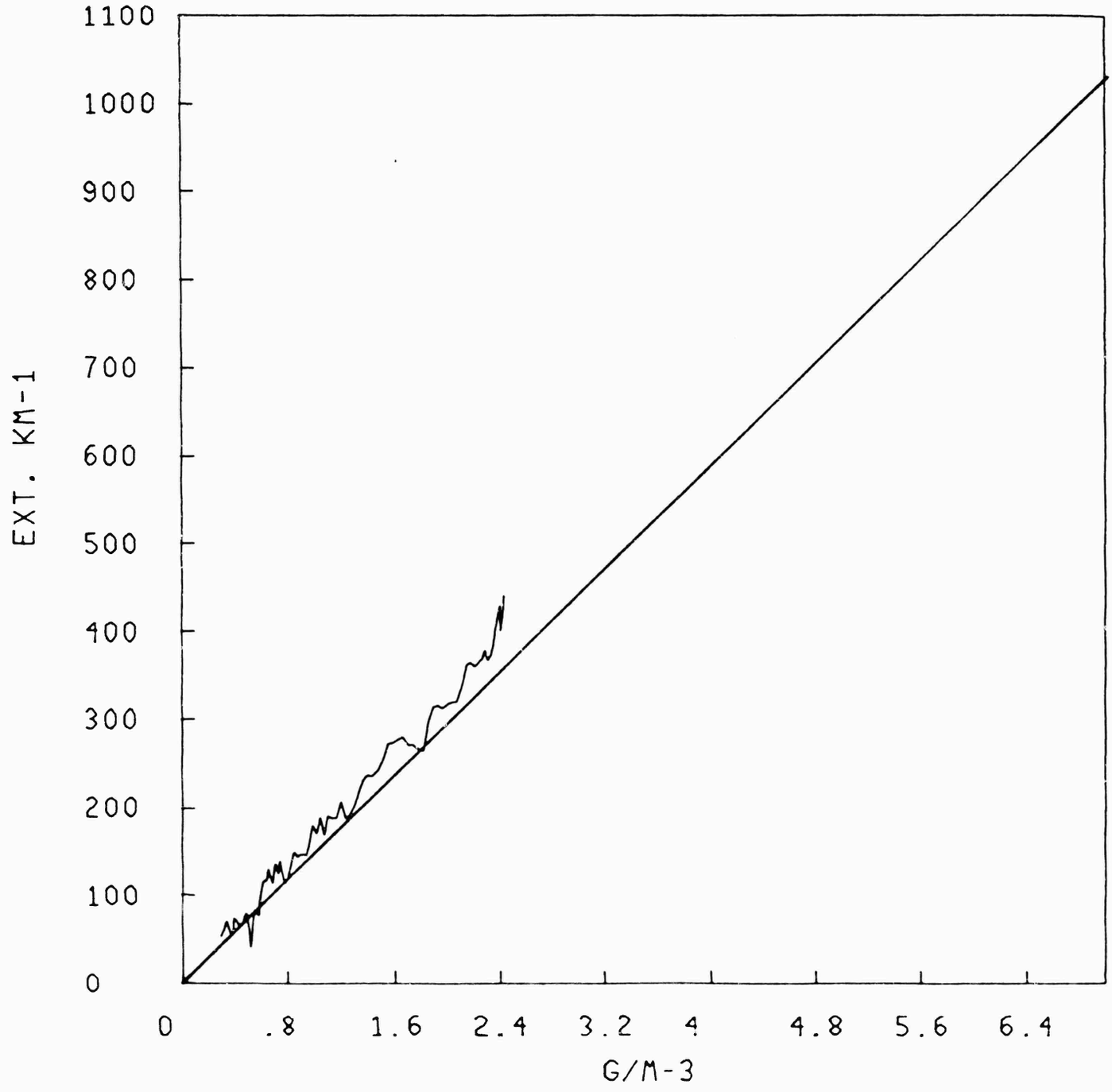

Fig. 2.1 Mie theory response calculations for the Knollenberg CSASP particle counter for NaCl particles (lighter curve) and water droplets.

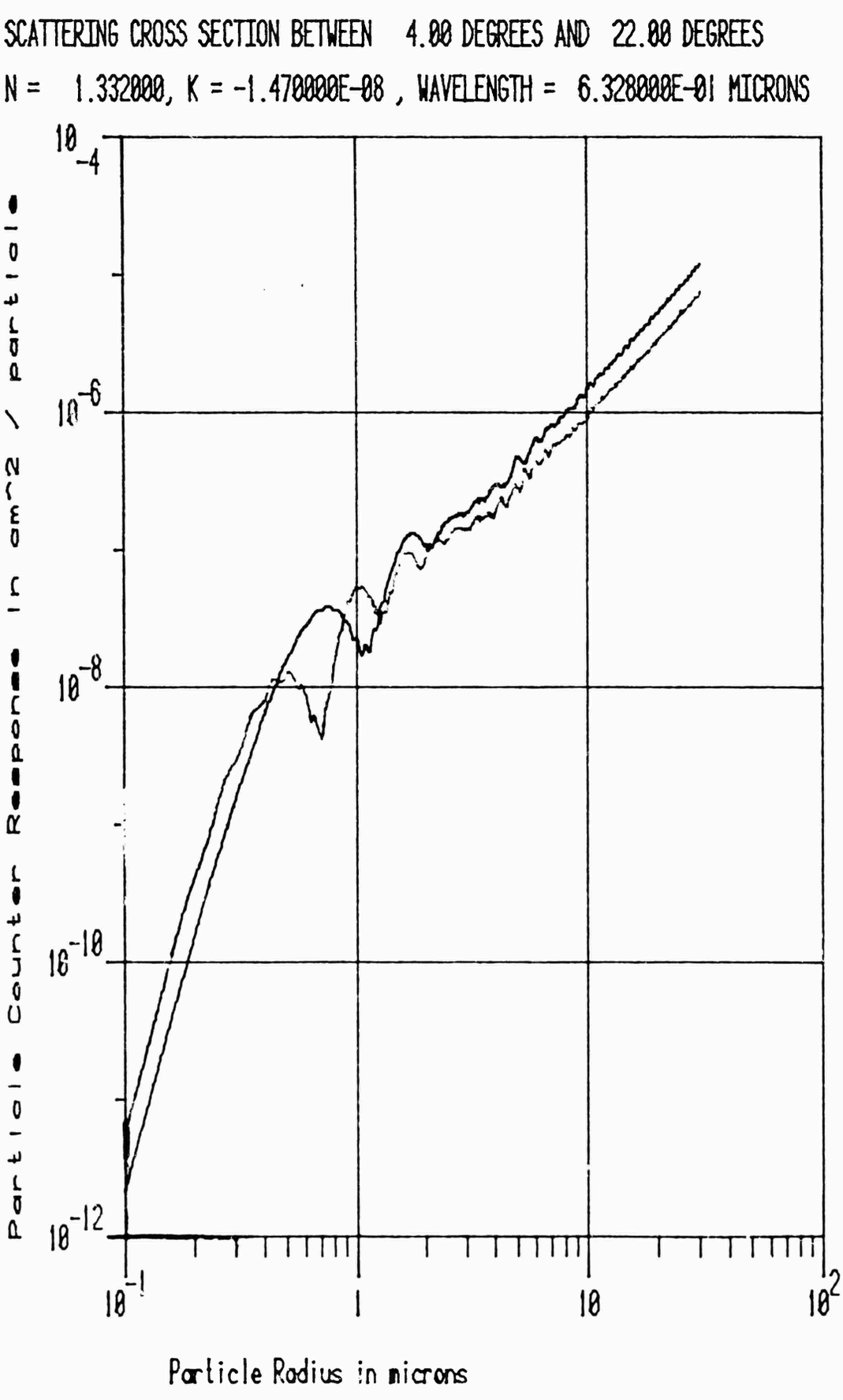

Fig. 2.2 Volume extinction coefficient at λ=10.6 μm versus liquid water content for 156 cloud droplet size distribution measurements of cumulus and stratus clouds.

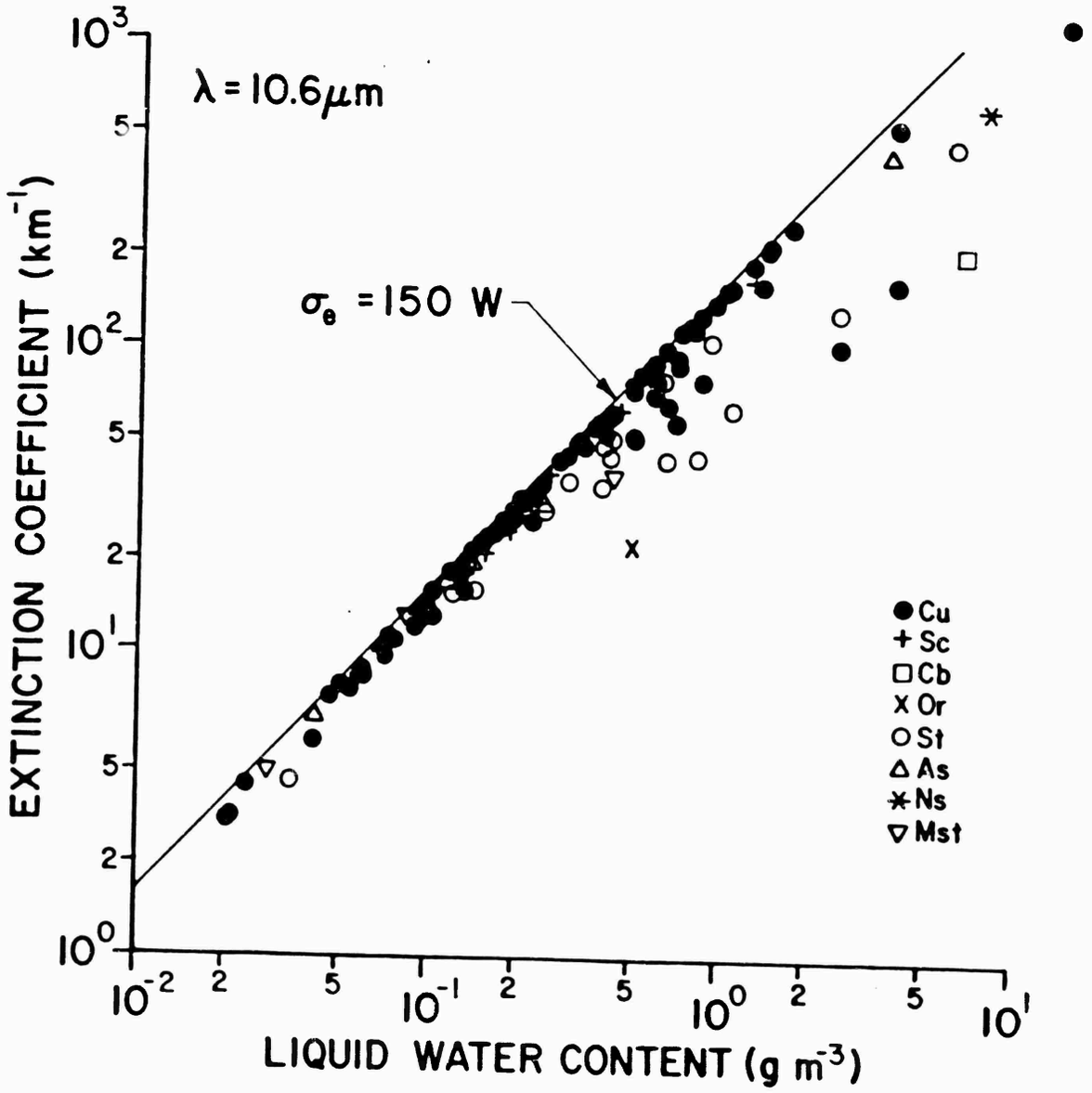

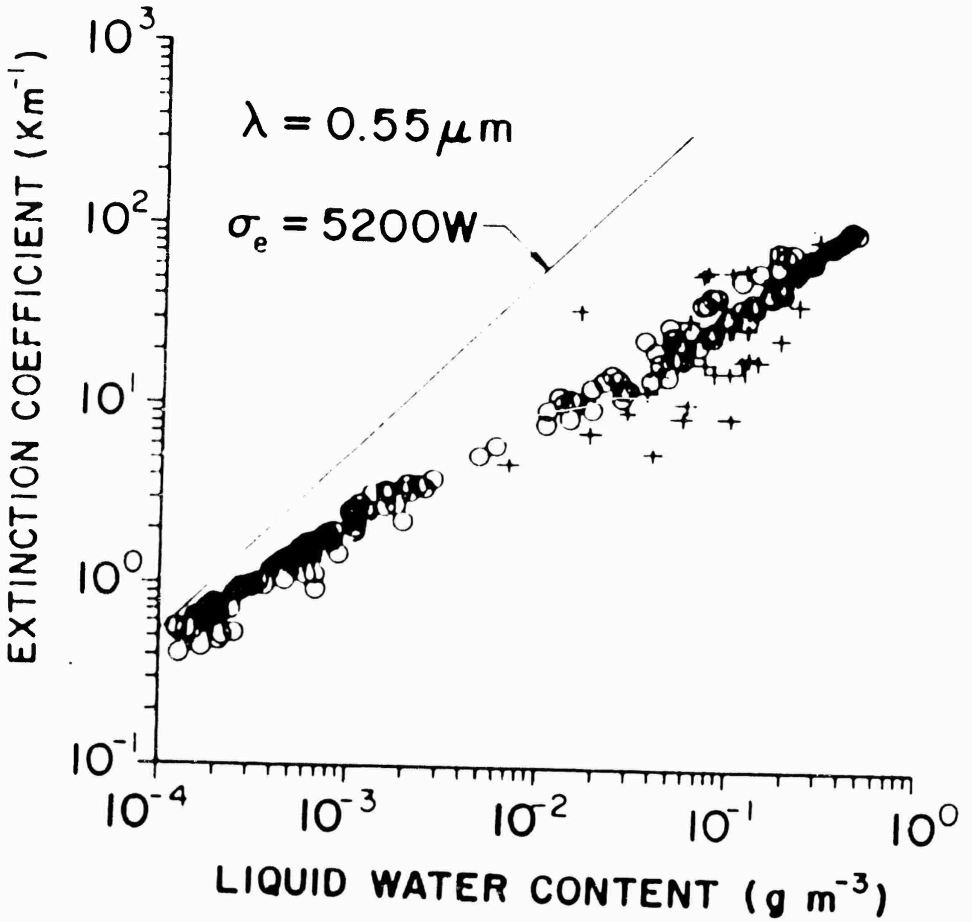

Fig. 2.3 Variation of extinction coefficient with liquid water content in atmospheric fog and haze for 320 size distribution measurements made at different geographic locales and under a variety of meteorological conditions.

Fig. 2.4 Volume extinction coefficient versus volume backscatter coefficient at wavelength λ = 1.06μm for 156 droplet size distributions measured for the major cloud types.

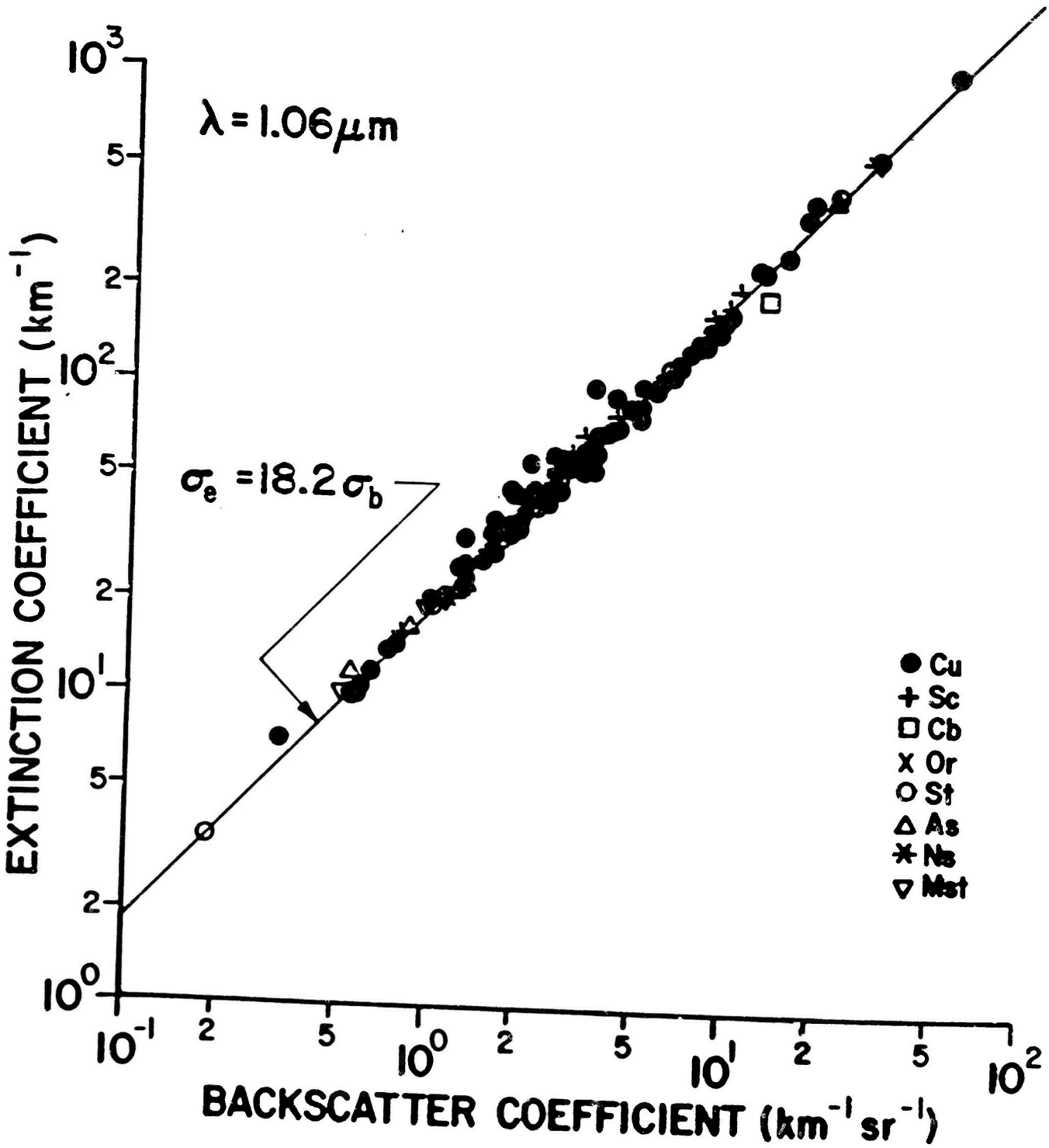

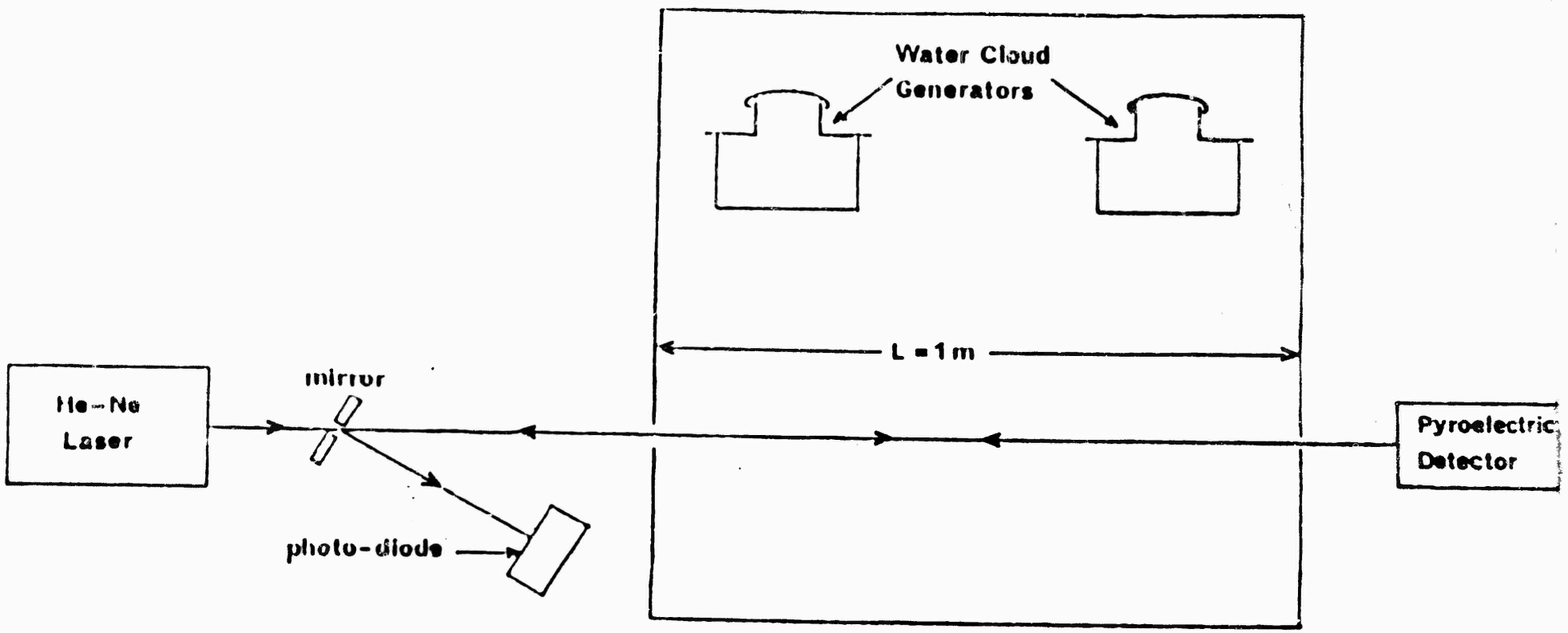

Fig. 2.5 Schematic diagram of the experimental system used to measure extinction and backscatter coefficient in laboratory cloud.

Fig. 2.6 Comparison of measured cloud backscatter and extinction coefficients with the theoretical relation (2.5).

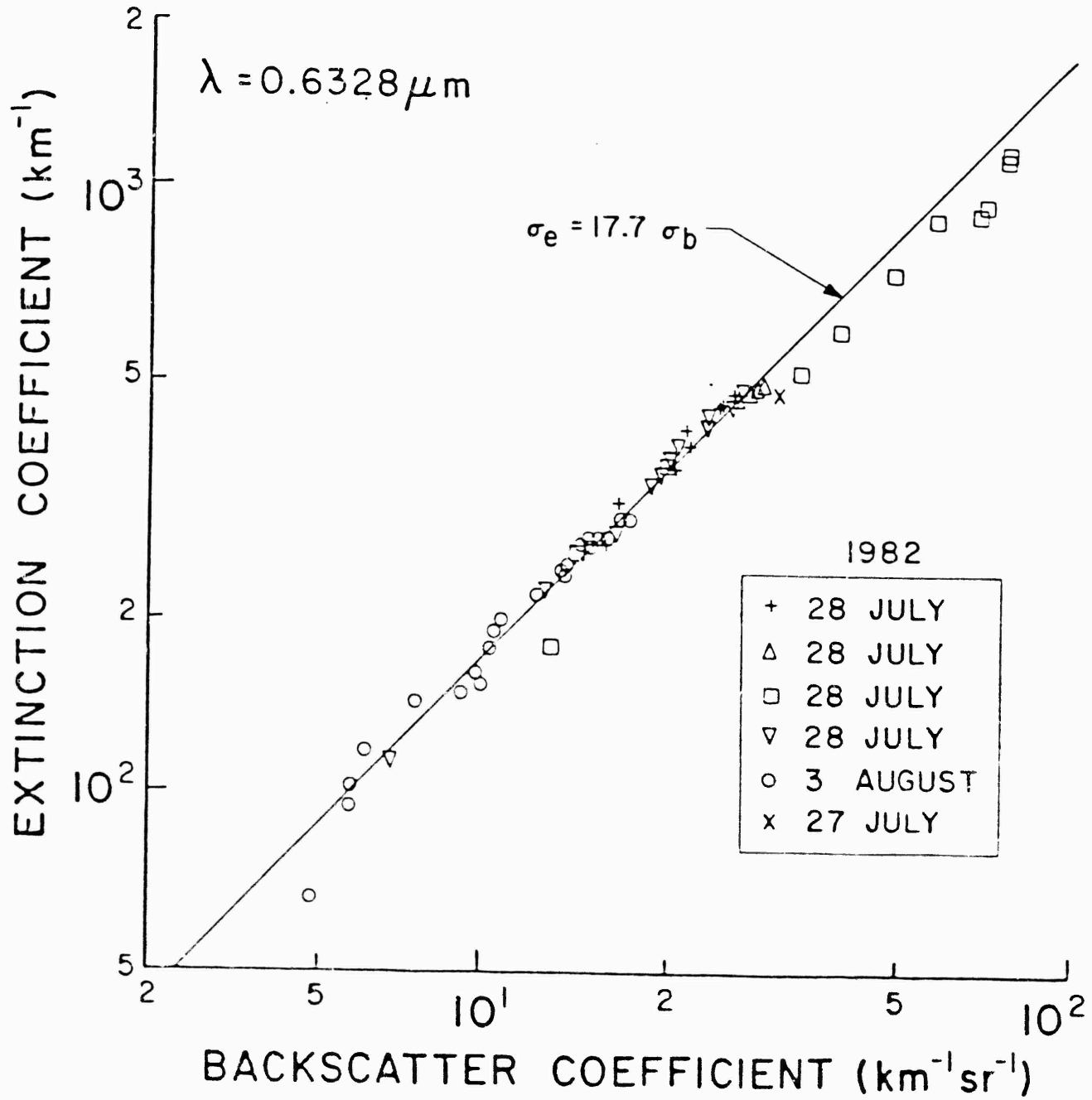

Fig. 2.7 Comparison of measured cloud extinction and backscatter coefficients with the theoretical prediction (2.5)

O : indicates measurements during buildup of cloud

● : indicates measurements during cloud decay.

The extinction and backscatter coefficient measurements were made for laboratory-generated clouds having an averaged size distribution shown in Fig. 1.3.

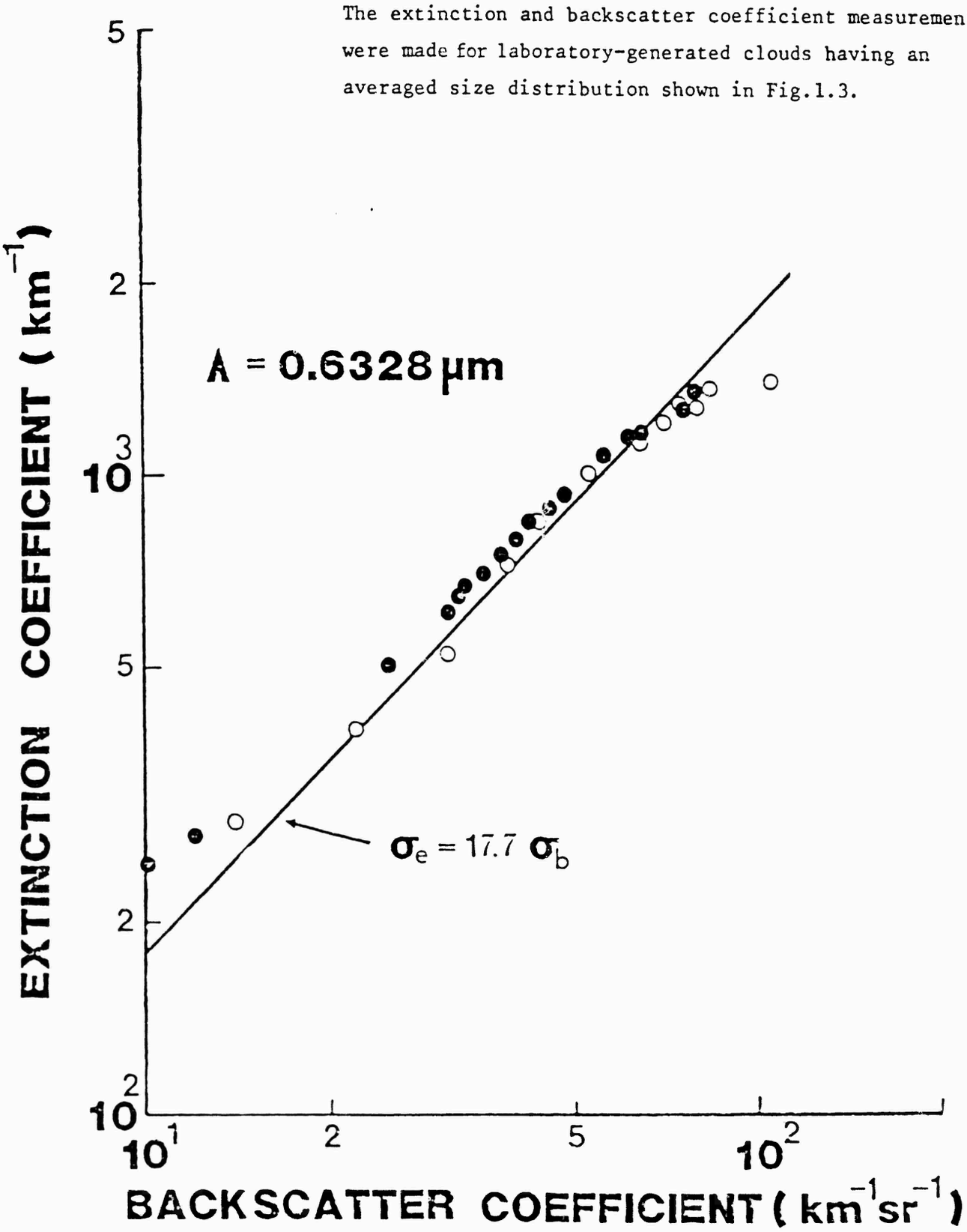

Fig. 2.8 As in figure 2.7 except for higher cloud nebulizer output.

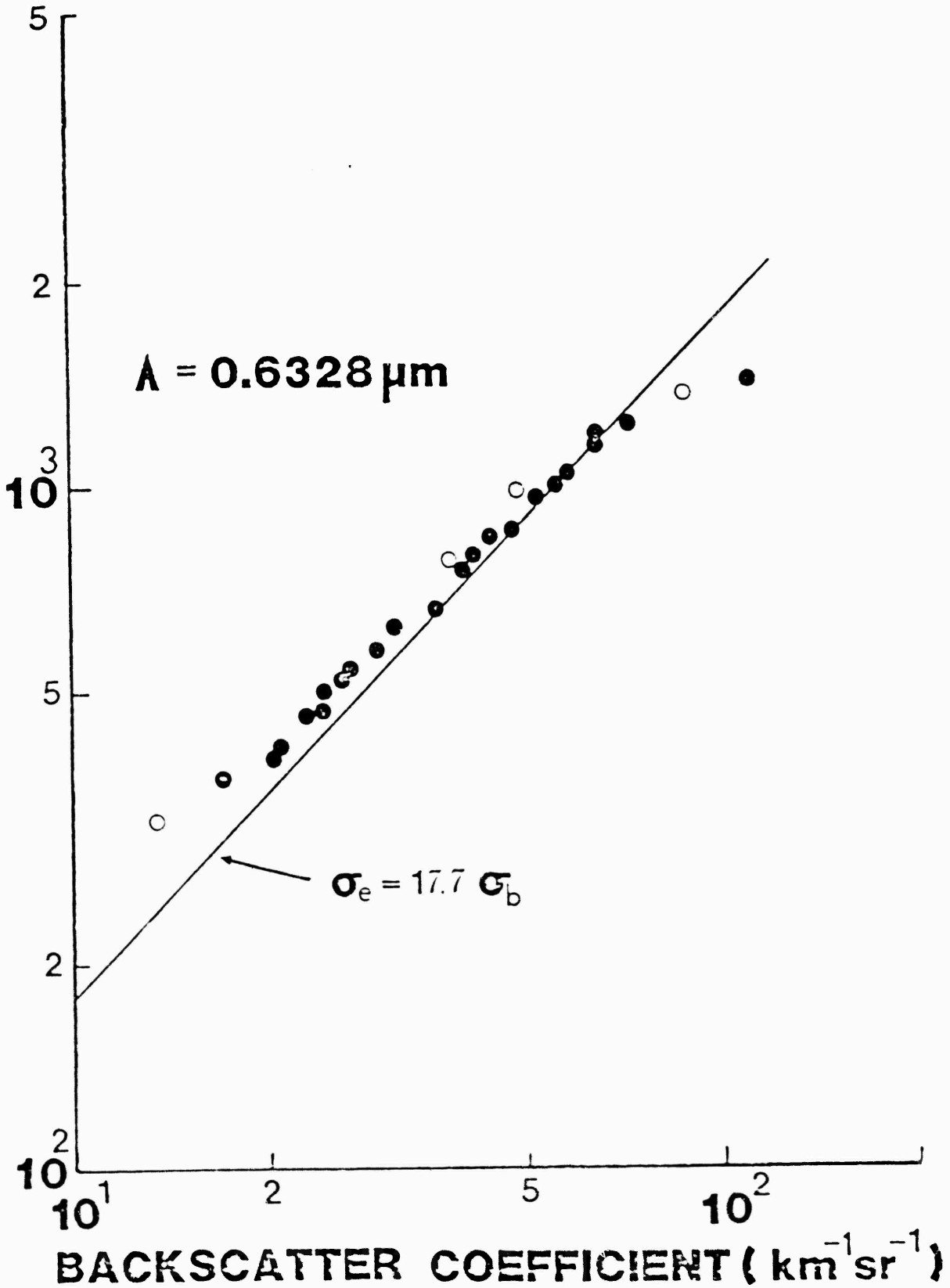

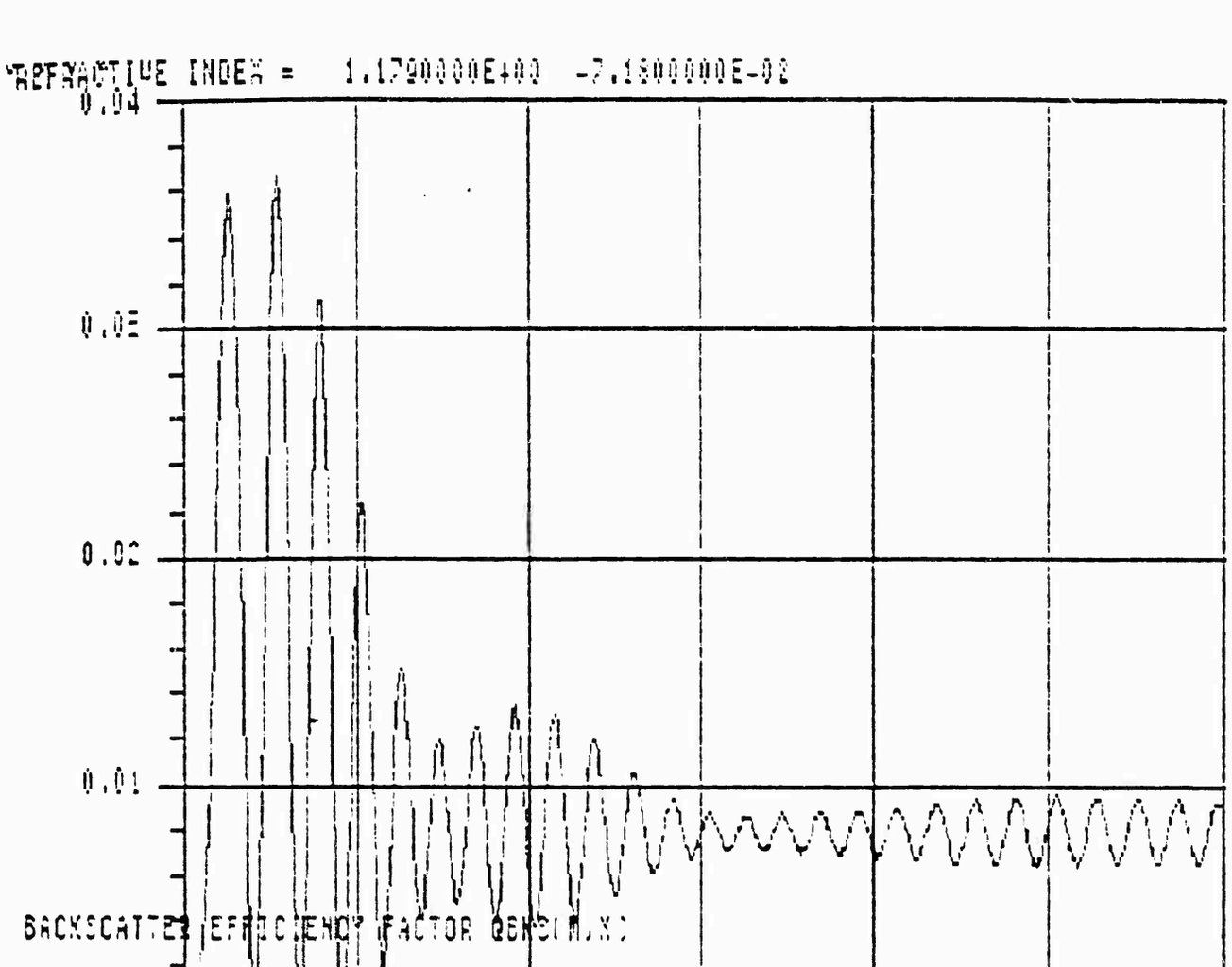

Fig. 3.1 Normalised backscatter cross-section as a function of size parameter x for water at wavelength λ = 10.591 micrometres.

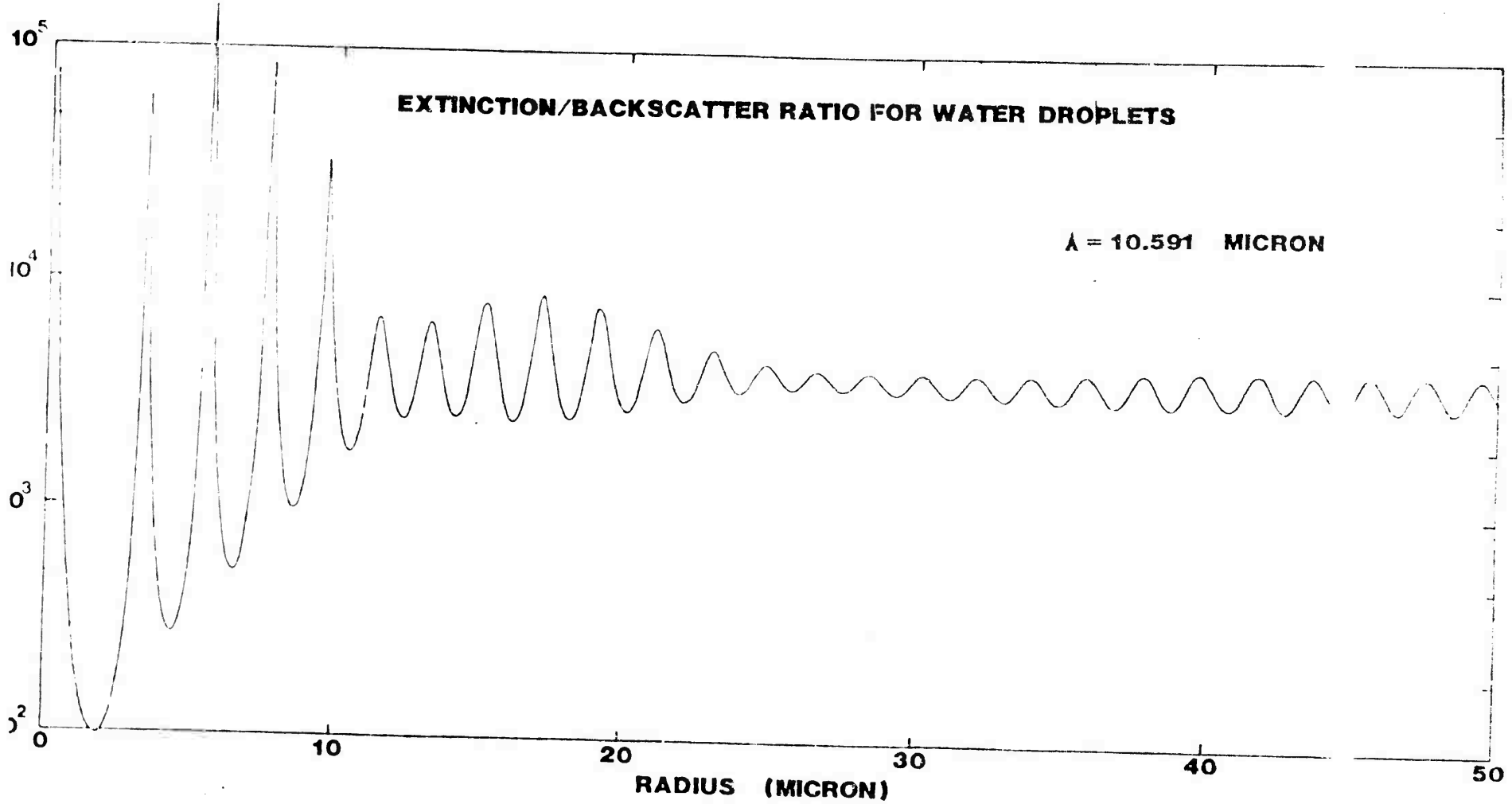

Fig. 3.2 Extinction to backscatter ratio for water droplets for wavelength $\lambda = 10.591$ μm.

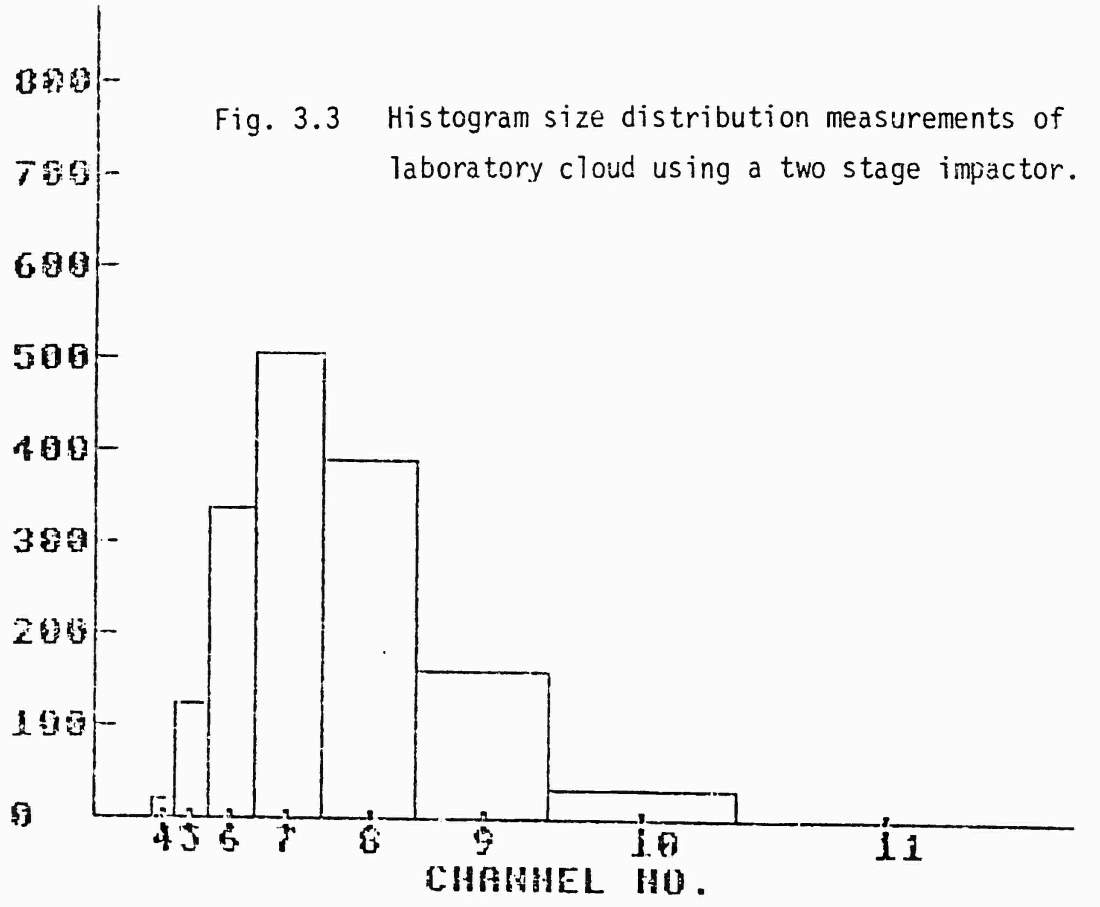

Fig. 3.3 Histogram size distribution measurements of laboratory cloud using a two stage impactor.

KEY TO CHANNEL NOS : (*10^-6M) DIAMETER

4 = 8.5 - 12.05
5 = 12.05 - 17.05
6 = 17.05 - 24.1
7 = 24.1 - 34.1
8 = 34.1 - 48.25
9 = 48.25 - 68.2
10 = 68.25 - 96.5
11 = 96.5 - 141.5

RESULTS FROM FLIGHT 46 25 1733 WITH DEHUMIDIFIER SETTING AT MED AND WIND TUNNEL POSITION AT 2N/3

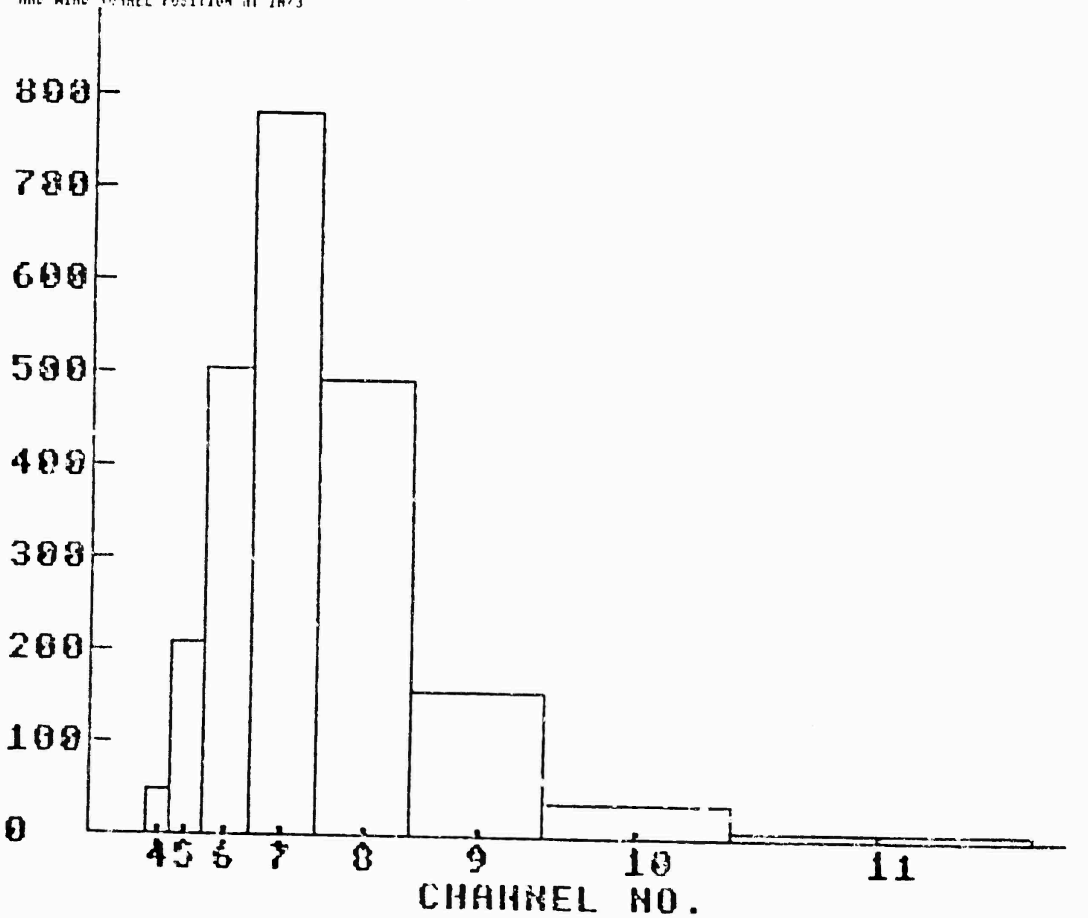

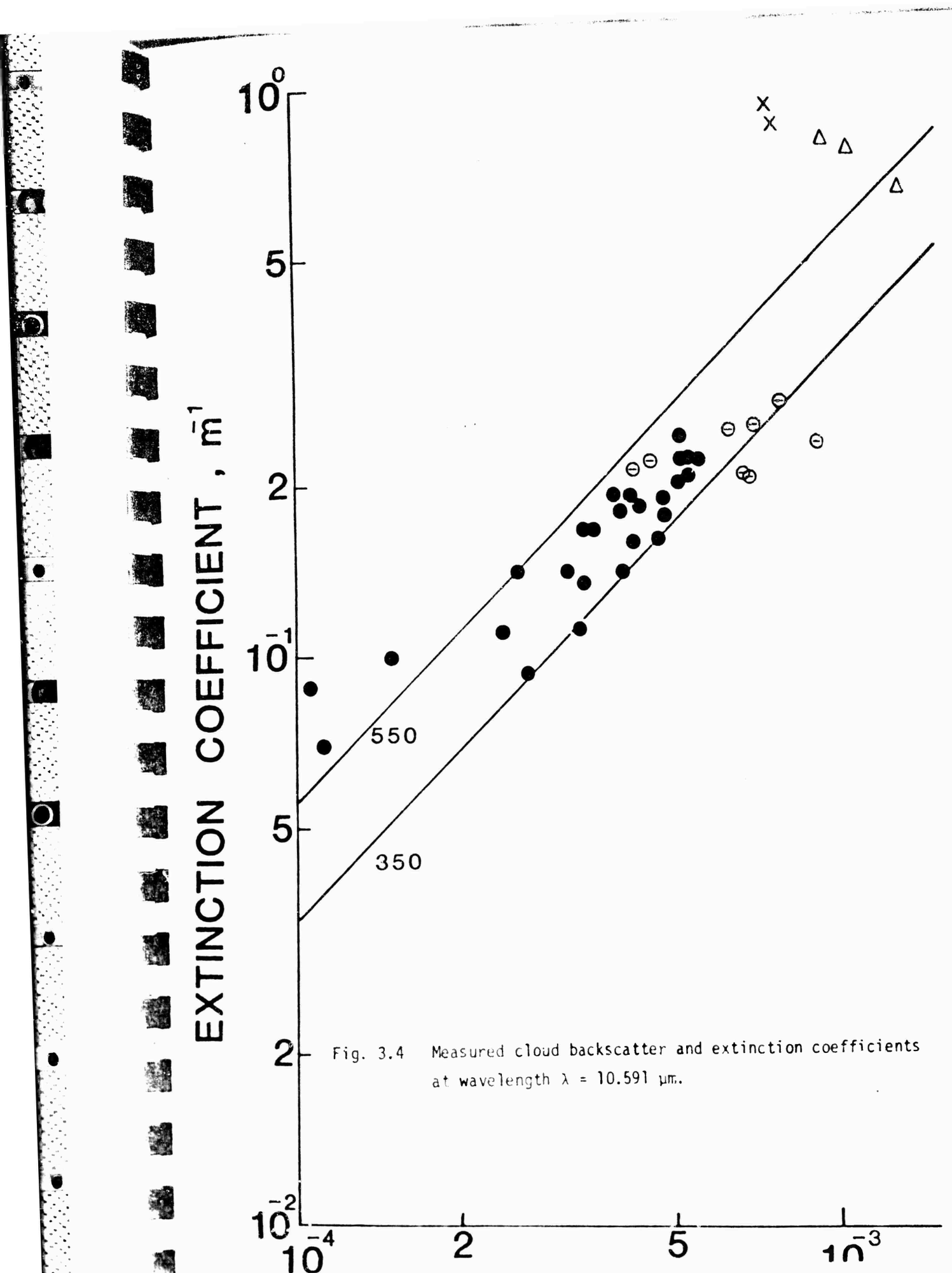

Fig. 3.4 Measured cloud backscatter and extinction coefficients at wavelength λ = 10.591 μm.

TABLE 1.1

Comparison of 2 filtration techniques for liquid water content measurement of cloud

Cloud Generator	Mass (g) using vertical filtration tube	Mass (g) using reference tube	Net mass of water (g)	Flow rate ℓ mm^{-1}	Sampling time S	Mass of cloud using top-balance (g)	Direct Filtration Mass / Top-balance mass
2 Humidifiers medium setting	0.063	0.016	0.047	8	117.7	0.039	1.17
" "	0.555	0.013	0.042	8	117.7	0.037	1.11
" "	0.055	0.016	0.039	8	117.4	0.040	0.98
2 Humidifiers high setting	0.102	0.016	0.086	5	174.8	0.074	1.16
" "	0.102	0.014	0.088	5	175.7	0.064	1.37
" "	0.100	0.013	0.087	5	175.7	0.064	1.36
		Replaced top-balance filter and restarted cloud					
" "	0.092	0.013	0.079	10	98.4	0.082	0.96
" "	0.100	0.009	0.091	10	98.0	0.079	1.16
		Replaced filter in top-balance assembly					
" "	0.103	0.019	0.084	10	98.2	0.080	1.05
" "	0.112	0.017	0.094	10	98.6	0.085	1.10
" "	0.107	0.016	0.091	10	98.5	0.077	1.19
		Dry filter replaced in top-balance assembly					
" "	0.102	0.021	0.081	10	98.3	0.081	1.00
2 Humidifiers low setting	0.075	0.009	0.066	10	98.4	0.069	0.96

APPENDIX 1

Backscatter and Extinction in Water Clouds

R.G. Pinnick, S.G. Jennings, Petr Chylek, C. Ham and
W.T. Grandy, Jr.

J. Geophy. Res., 88, pp. 6787-6796, 1983.

JOURNAL OF GEOPHYSICAL RESEARCH, VOL. 88, NO. C11, PAGES 6787–6796, AUGUST 20, 1983

Backscatter and Extinction in Water Clouds

R. G. PINNICK,[1] S. G. JENNINGS,[2] PETR CHÝLEK,[3] CHRIS HAM,[4] AND W. T. GRANDY, JR.[5]

An approximate relation between the volume extinction coefficient σ_e and backscatter coefficient σ_b of atmospheric cloud at visible and near-infrared wavelengths is derived. The relation is only weakly dependent on the size distribution of droplets and has the form $\sigma_e/\sigma_b = (8\pi/g)\{1 + k^{-2/3}(\langle r^{4/3}\rangle/\langle r^2\rangle) - \delta[k^2(\langle r^4\rangle/\langle r^2\rangle) + k^{4/3}(\langle r^{4/3}\rangle\langle r^4\rangle/\langle r^2\rangle\langle r^2\rangle)]\}$ where the extinction efficiency is approximated by a complex-angular-momentum-theory result and the parameters g and δ are determined by approximating a running mean of the backscatter gain by $G(x) = g(1 + \delta x^2)$ (x is droplet size parameter and $\delta \ll 1$), k is the wave number, and $\langle r^n\rangle$ is the nth moment of the droplet size distribution. To zero order the relation is linear and independent of the droplet size distribution $\sigma_e = [8\pi/g(\lambda)]\sigma_b$ where $g(\lambda)$ is a slowly varying function of wavelength. At a wavelength $\lambda = 1.06$ μm the relation is σ_e (km^{-1}) = 18.2 σ_b (km^{-1} sr^{-1}). Predictions made with this simple zero-order approximation are in good agreement (within 50%) with Mie calculations of extinction and backscatter coefficients based on 156 measurements of cloud droplet spectra in cumulus and stratus type clouds. The linear $\sigma_e - \sigma_b$ relation is also in agreement with extinction and backscatter measurements made on laboratory-generated fog droplet distributions. The relation suggests that visible or near-infrared extinction coefficients in cloud of unknown type could be inferred from lidar backscatter measurements alone, without knowledge of the cloud droplet size spectra, barring complications arising from multiple scattering contributions to the lidar return.

1. INTRODUCTION

A possible relation between atmospheric backscatter and extinction (or visibility) has been of interest to scientists for more than 2 decades. *Curcio and Knestrick* [1958] found experimentally by using a white light source a definite correlation between backscatter and transmission measurements for atmospheric conditions ranging from relatively clear weather to fog to drizzle. *Twomey and Howell* [1965] were able to at least partially explain Curcio's findings by showing that for polydispersions of water droplets the ratio of calculated particle backscatter to extinction for a white light source is only a weak function of droplet size distribution. They used Gaussian, Poisson, reversed Poisson, and bimodal distributions characteristic of atmospheric fog and haze in their numerical study. Additional experimental evidence for correlation of backscatter and extinction for white light sources was provided by *Vogt* [1968].

With the coming of the laser used in the lidar technique and its application to the remote measurement of cloud [*Collis*, 1965; *Schotland et al.*, 1971; *Plass and Kattawar*, 1971; *Zuev and Balin*, 1972; *Platt*, 1973; *Derr et al.*, 1976; and others] there was additional interest in the question of a possible relation between backscatter and extinction, but in this case for monochromatic sources. Although *Silverman and Sprague* [1970] did not intend to utilize a laser source in their instrument for single-ended measurements of visibility, their feasibility studies are for monochromatic sources. They calculated the backscatter coefficient σ_b and the extinction coefficient σ_e for polydispersions of water droplets having gamma-type size distributions considered to be characteristic of common fog and cloud types. Their numerical studies indicate an approximate relation between backscatter and extinction of the form $\sigma_e \sim \sigma_b^{0.90}$. Similar numerical investigations, but specifically for the lidar application, have been made by *Derr* [1980]. Derr showed the backscatter to extinction ratio for ruby ($\lambda = 0.694$ μm) and Nd-YAG ($\lambda = 1.06$ μm) sources is a slowly varying function of drop size. Like Silverman, Derr calculated backscatter to extinction ratios averaged over various gamma size distributions representative of cumulus and cumulonimbus cloud and from these results estimated approximate linear relations between backscatter and extinction coefficients.

Up to this point, then, investigators have found either experimentally or through numerical studies that there should exist at least an approximate relation between backscatter and extinction coefficients in water clouds, but the underlying reason for the relation is unclear.

In this paper we re-examine from a theoretical standpoint, in light of recent complex-angular-momentum theory predictions [*Nussenzveig*, 1969; *Khare and Nussenzveig*, 1977*a*; *Nussenzveig and Wiscombe*, 1980], the question of a possible relation between backscatter and extinction, and the universality such a relation might have.

We derive, using a complex-angular-momentum theory approximation for the extinction efficiency, and a simple curve-fit approximation for the running mean of the backscatter gain, a relation between extinction and backscatter that to zero order is independent of droplet size distribution; higher-order terms in our solution take the size distribution dependence into account. These terms are worked out explicitly for gamma-type size distributions characteristic of cloud and are found to contribute on the order of 10% of the leading term. Because of the simple form of the solution which neglects higher-order terms (wherein extinction is related linearly to backscatter with no size distribution dependence), we concentrate on investigating the universality of this (zero order) solution. We compare the zero order solution (which at $\lambda = 1.06$ μm is σ_e (km^{-1}) = 18.2 σ_b (km^{-1} sr^{-1})) to both Mie calculations (for 156 measured droplet distributions) and measurements of backscatter and extinction made on laboratory generated clouds. Agreement is in both cases generally within 50%. Our experimental verification of this linear $\sigma_e - \sigma_b$ relation is the first such work that is definitive.

[1] U.S. Army Atmospheric Sciences Laboratory, White Sands Missile Range, New Mexico 88002.
[2] Department of Physics, University College, Galway, Ireland.
[3] Atmospheric Sciences Research Center, State University of New York in Albany, Albany, New York 12222.
[4] Physical Sciences Laboratory, New Mexico State University, Las Cruces, New Mexico 88003.
[5] Department of Physics and Astronomy, University of Wyoming, Laramie, Wyoming 82071.

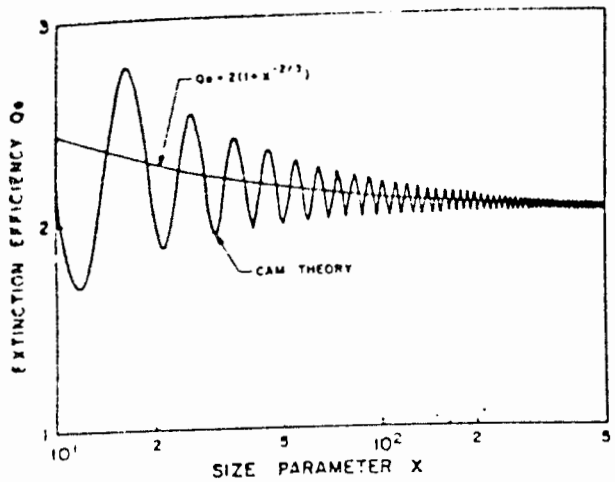

Fig. 1. Complex angular momentum (CAM) theory calculations of the extinction efficiency for water droplets having size parameters characteristics of water cloud (at visible and near-IR wavelengths). Also shown are results for the lowest order CAM theory terms used in the derivation of the backscatter-extinction relation (17).

relation exists at an infrared laser (10.6 μm) wavelength, where the backscatter to extinction ratio can vary by more than an order of magnitude with the form of the cloud droplet size distribution. We also show that cloud liquid water content for clouds of unknown droplet size distribution cannot be inferred from visible, infrared, or near-millimeter backscatter measurements alone. Finally, we demonstrate that previously derived relations between infrared ($\lambda = 10.6$ μm) extinction and liquid water content in fog, and between infrared ($\lambda = 3.8$ μm) absorption and liquid water content in fog [*Chýlek*, 1978; *Pinnick et al.*, 1979] can also be applied to most clouds.

2. Backscatter and Extinction in Cloud

The volume extinction and backscatter coefficients σ_e and σ_b of a polydispersion of spherical cloud droplets characterized by a size distribution $n(r)$ and refractive index m are given by

$$\sigma_e = \int \pi r^2 Q_e n(r)\, dr \tag{1}$$

$$\sigma_b = \frac{1}{4\pi} \int \pi r^2 G n(r)\, dr \tag{2}$$

where $Q_e(m, x)$ is the Mie efficiency factor for extinction for a particle with refractive index m and size parameter $x = 2\pi r/\lambda$, and $G(m, x)$ is the backscatter gain defined as 4π times the ratio of the backscatter differential cross section to the geometric area. Because of the complex size dependence of Q_e and G, if we are to find an approximate relation between extinction and backscatter coefficients, we will no doubt have to resort to some approximate expressions for the Mie efficiencies Q_e and G in equations (1) and (2).

3. Approximation for the Extinction Efficiency

Extinction in cloud is dominated by droplets with radii 2 μm $< r <$ 85 μm, corresponding to size parameters $12 < x < 500$ at a wavelength $\lambda = 1.06$ μm. These relatively large size parameter values suggest asymptotic expansions for the Mie extinction and backscatter efficiencies, and just such a theory has been developed by *Nussenzveig* [1969], who analytically continued the Mie series into the complex angular momentum plane. The resulting analytic expressions for the scattering functions, for large x, are given in terms of the poles and saddle points contributing to the scattering amplitudes in the complex plane of summation index. The complex-angular-momentum (CAM) theory expression for the extinction efficiency has been worked out by *Nussenzveig and Wiscombe* [1980]:

$$Q_e = 2 + 1.992x^{-2/3} - \frac{8m^2}{(m^2 - 1)(m + 1)} \sin\,[2(m - 1)x]x^{-1} - 0.715x^{-4/3} + O(x^{-5/3}) \tag{3}$$

A plot of this approximate expression for Q_e (Figure 1) shows the familiar damped oscillating behavior with period $\Delta x = \pi/(m - 1) \cong 9.5$. If we can assume atmospheric cloud droplets generally have slowly varying concentrations over corresponding radius intervals ($\Delta r = 1.6$ μm at $\lambda = 1.06$ μm), then, since we are concerned only with integrals of Q_e over cloud size distributions, we can neglect the oscillatory sin term in (3). We can also neglect the terms $O(x^{-4/3})$ and $O(x^{-5/3})$ since for $x > 10$ they are less than ~10% of the second term $O(x^{-2/3})$. Given these constraints we can approximate Q_e by

$$Q_e = 2(1 + x^{-2/3}) \tag{4}$$

as shown in Figure 1.

4. Approximation for the Backscatter Gain

The backscatter cross section (and backscatter gain) can also be approximated by using complex-angular-momentum theory. Within the framework of CAM theory the single-particle backscatter cross section

$$\sigma_b' = \pi r^2 G = \frac{4\pi}{k^2}\left|S_1(x, \pi)\right|^2 \tag{5}$$

is evaluated by making a Debye expansion of the scattering matrix [*Nussenzveig*, 1979]

$$S_j(x, \pi) = \sum_{p=0}^{\infty} S_{j,p}(x, \pi) \qquad j = 1, 2 \tag{6}$$

and identifying dominant terms. In this expansion the pth term is associated with $(p - 1)$ internal reflections at the droplet surface, except for $p = 0$, which is associated with direct reflection. According to the computer evaluations of Khare and Nuzzenzveig [*Nussenzveig*, 1979] for water droplets with index of refraction given by

$$n = [\cos\,(11\pi/48)]^{-1} = 1.33007 \tag{7}$$

the following four-term approximation to the amplitudes accounts for 80–90% of the backscattered intensity

$$S_j(x, \pi) = S_{j,2}^{(\text{res})} + S_{j,11}^{(R)} + S_{j,0}^{(g)} + S_{j,2}^{(g)} \tag{8}$$

These arise from the ($p = 2$) residue series, the 10th-order rainbow, and the geometrical optics rays at $p = 0$, $p = 2$. The intensity computed from (8), $|S_j|^2$, gives rise to interference among the four terms, resulting in quasiperiodic oscillations with periods $\Delta x = 0.41$, 0.83, 1.1, 14 [*Nussenzveig*, 1979]. These periods are evident in Mie calculations of the backscatter gain in Figure 2.

Since our interest is in backscattering from a polydispersion of many cloud droplets of different size, rather than backscattering from single droplets, we are motivated to consider averages of the intensity. If one averages over the largest period, $\Delta x = 14$, the intensity in the backward direction is well

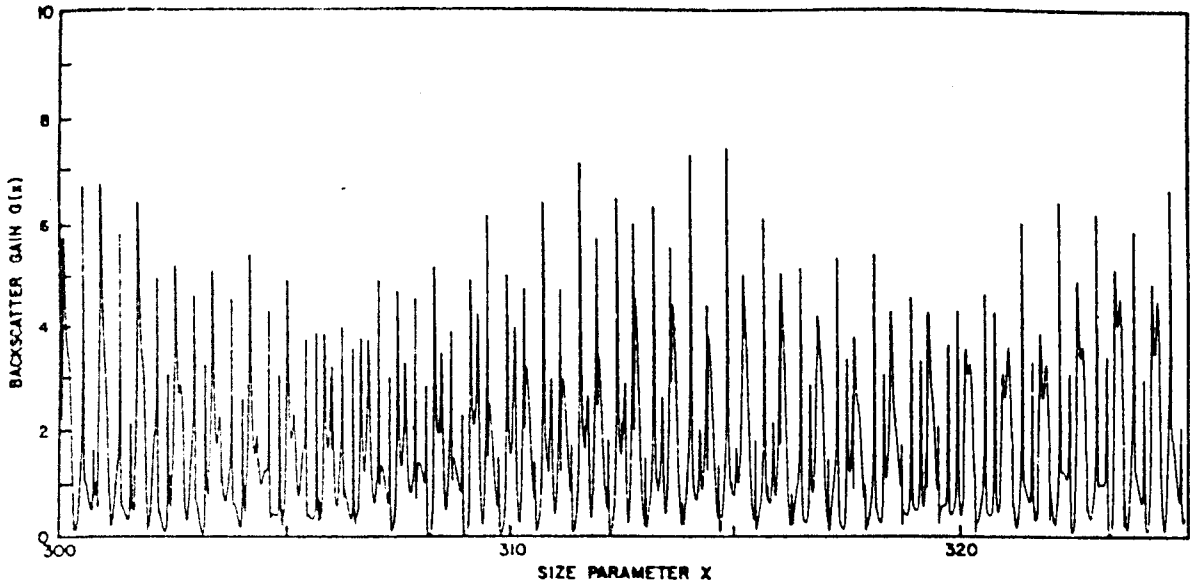

Fig. 2. Mie calculations of the backscatter gain $G(x)$ for water droplets at a wavelength $\lambda = 1.06$ μm (refractive index $m = 1.325 - 5 \times 10^{-3}i$) calculated for size parameters around $x = 300$ with resolution in size parameter $\Delta x = 0.01$. The quasiperiodic structure with periods $\Delta x \cong 0.41, 0.83, 14$ are apparent.

approximated by the sum of the squares of the amplitudes on the right-hand side of (8). Moreover, the geometrical optics terms are $O(x)$ and make small contributions in the range $20 < x < 500$. Thus, for our purposes (water drops in cloud),

$$|S_j(x, \pi)|^2 = |S_{j,2}^{(res)}(x, \pi)|^2 + |S_{j,11}^{(R)}(x, \pi)|^2 \qquad (9)$$

and only the $p = 2$ residue series and $p = 11$ (10th-order rainbow) Debye terms of the scattering amplitude need be evaluated.

The following asymptotic expressions for these terms can be extracted from *Khare*'s [1976] thesis

Tenth-Order Rainbow ($p = 11$)

$$S_{1,11}^{(R)}(x, \pi) = \pi m \kappa^{5/3} \exp(\kappa A)[p_0^E - p_0^M) Ai(\kappa^{2/3}\zeta) - \kappa^{-1/3}(q_0^E - q_0^M) Ai'(\kappa^{2/3}\zeta)] \qquad (10)$$

Where $\kappa = 2x$, the parameters A, ζ, p_0^E, p_0^M, q_0^E, and q_0^M are determined by saddle point evaluations in the complex angular momentum plane [*Khare and Nussenveig*, 1977*b*], and Ai is the Airy function [*Abramowitz and Stegun*, 1966]. Evaluation of these parameters leads to the following expression for the 10th-order rainbow term

$$|S_{1,11}^{(R)}(x, \pi)|^2 = 175.99x^{10/3}[9.8 \times 10^{-7}|Ai(-0.00411x^{2/3})|^2 + 1.37 \times 10^{-5}x^{-2/3}|Ai'(-0.00411x^{2/3})|^2] \qquad (11)$$

Residue Series ($p = 2$)

Once again we extract from Khare's thesis the leading behavior of this term:

$$S_{1,2}^{(res)}(x, \pi) = -0.24276x^{4/3}\exp(-0.42074x^{1/3}) \cdot \exp[i(2m\kappa - \pi/6 + x\zeta_2)] \qquad (12)$$

where ζ_2 is a small purely real angle. Finally, squaring this amplitude gives

$$|S_{1,2}^{(res)}(x, \pi)|^2 = 0.05893x^{8/3}\exp(-0.8415x^{1/3}) \qquad (13)$$

The CAM theory result for the backscatter gain, calculated according to equations (5), (9), (11), and (13)

$$G(x) = 704x^{4/3}[9.8 \times 10^{-7}|Ai(-0.00411x^{2/3})|^2 + 1.37 \times 10^{-5}x^{-2/3}|Ai'(-0.00411x^{2/3})|^2] + 0.236x^{2/3}\exp(-0.842x^{1/3}) \qquad (14)$$

are shown compared to the exact Mie result (averaged over $\Delta x = 0.83$) in Figure 3.

Although the CAM theory prediction has the correct form (it is slowly varying over the range $20 < x < 500$, but nevertheless steadily increases for $x > 200$), it is too low by an additive constant of about 1.2. (As an aside we note that the geometrical optics ray contribution to the backscatter gain has the correct form to account for this discrepancy, but it is still small compared to the terms in (14).) We offer the following reasons for the underprediction by CAM theory: (1) We have retained only leading order corrections in the asymptotic expansions of the $p = 2$, 11 terms in the Debye series, and (2) there is no apparent fundamental reason for the existence of a unique functional relation between backscattering and extinction coefficients, for they correspond to entirely different physical processes. That the theory nevertheless provides qualitatively correct verification of our expectations is remarkable, and thus the connection seems worthy of further analysis. We leave this further analysis for future work.

Because of our failure to reproduce the correct magnitude result with CAM theory, we instead propose a simple curve-fit approximation to the backscatter gain. Since our interest is in lidar backscattering from a polydispersion of droplets (rather than from single droplets) we again neglect the oscillatory component evident in the exact Mie results and approximate the gain by

$$G(x) = g(\lambda)(1 + \delta x^2) \qquad (15)$$

where $g(\lambda)$ is a slowly varying function of wavelength and $\delta \ll 1$. This approximate expression is shown compared to the exact Mie results in Figure 3.

TABLE 2. Cloud Size Distribution Measurements

Source	Cloud Type	Range of Droplet Sizes Measured (radii in μm)	Number of Drop Size Distribution Measurements
aufm Kampe and Weickmann [1952]	Cumulus Congestus	1.5–92	1
Battan and Reitan [1957]	Cumulus Cumulus Congestus Tropical Cumulus	1.75–58	5
Diem [1948]	Cumulus Cumulus Congestus Stratocumulus Altostratus Nimbostratus Stratus	1–42	6
Durbin [1959]	Cumulus	0.75–30	22
Eagan et al. [1974]	Stratocumulus Cumulus	1.25–15	12
Fitzgerald [1972]	Continental Cumulus Maritime Cumulus	3.5–11.5	7
Fitzgerald and Spyers-Duran [1973]	Cumulus Stratocumulus	1.75–10.5	4
Jiusto [1967]	Maritime Cumulus Orographic Stratocumulus	1.5–24	4
Ryan et al. [1972]	Continental Cumulus Maritime Stratus Maritime Cumulus	2–42	33
Singleton and Smith [1960]	Stratus	1.5–62	17
Spyers-Duran [1972]	Altostratus Altocumulus	2.5–24	8
Squires [1958]	Orographic Tradewind Cumulus Continental Cumulus	2.5–82	10
Warner [1969, 1973a]	Cumulus	1.25–24	20
Warner [1973b]	Maritime Cumulus	1.5–13	4
Weickmann and aufm Kampe [1953]	Cumulus Congestus Cumulonimbus	2.5–100	3

recipitation cloud model C.6. Although the series appears to e diverging for the C.6 model, this is not the case. In fact, for recipitating clouds the higher-order terms decrease rapidly in nagnitude and further partially cancel the term $O(\delta)$ in equations (17) and (19), rendering the leading term more dominant. his suggests that if ~20% errors are acceptable, equation 7) has a particularly simple form

$$\sigma_e = \frac{8\pi}{g}\,\sigma_b \tag{20}$$

here the extinction is a linear function of backscatter, indeendent of droplet size.

Of course, the argument that higher-order terms in (19) are mall assumes cloud droplet distributions are broad (so that he oscillatory terms in Q_e and G can be neglected) and further hat they have a single-mode gamma-type size distribution. his latter assumption in particular is not very realistic for all loud types. In the next section we investigate the range of alidity of the linear extinction-backscatter relation (20) for nore realistic (measured) cloud distributions.

6. Numerical Verification of the Extinction-Backscatter Relation

To test the range of validity of the linear extinction-backscatter relation (20) for cloud we calculated, using Mie

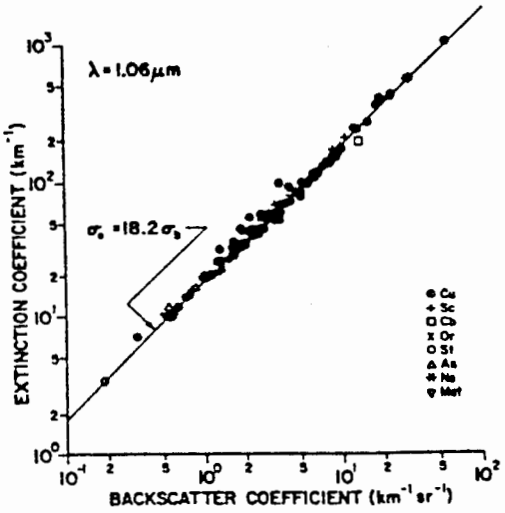

Fig. 4. Volume extinction coefficient versus volume backscatter coefficient at a wavelength $\lambda = 1.06$ μm for 156 droplet size distributions measured in the major cloud types: Cu, denotes cumulus, cumulus congestus, continental cumulus, maritime cumulus, tropical cumulus, altocumulus, and tradewind cumulus; Sc, stratocumulus; Cb, cumulonimbus; Or, orographic; St, stratus; As, altostratus; Ns, nimbostratus; and Mst denotes maritime stratus. The results are in good agreement with the size-distribution-independent prediction (20) (shown by the solid straight line) relating extinction uniquely to backscatter.

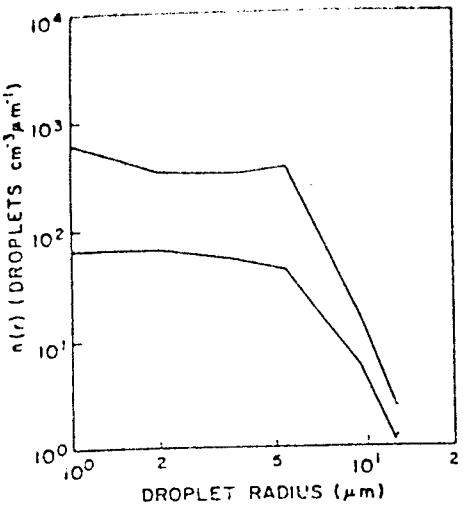

Fig. 5. Typical laboratory-generated cloud droplet distributions used to investigate the accuracy of the extinction-backscatter relation (20). The measurements were made with a model CSASP-100 light scattering counter (manufactured by Particle Measurement Systems, Inc., Boulder, Colo.) calibrated for water droplets according to the prescription of *Pinnick and Auvermann* [1979].

theory and indexes of refraction of water given by *Hale and Querry* [1973], the extinction coefficient according to equation (1) and the backscatter coefficient according to equation (2) for 156 cloud droplet size distributions measured in the major cloud types. The sources of these measurements together with the range of droplet sizes measured and other pertinent information is listed in Table 2. The main sampling technique employed to obtain the cloud droplet size distributions was that of impaction of droplets onto coated slides or replicators whose collection efficiencies were known. The practical lower limit for detection of cloud droplets by the impaction technique is around 1.5 μm radius. The sole cloud size determination by a light scattering counter [*Ryan et al.*, 1972] was calibrated by means of uniformly sized water droplets. Only nonprecipitating clouds were used in the analysis and measurements which showed evidence of glaciation were excluded.

The numerical calculations of extinction and backscatter are shown compared to our linear relation (20) in Figure 4 for $\lambda = 1.06$ μm. (As an aside we note that *Derr*'s [1980] relation between extinction and backscatter $\sigma_e = 18.0\,\sigma_b$ is negligibly different from our relation (20) at this wavelength.) For all considered cloud size distributions, the relation (20) is within 50% of the numerical results. If the measured droplet distributions were extrapolated beyond the range of measured sizes (imposed by the instrumentation), then the calculated extinction and backscatter coefficients would probably fall even closer to our relation (20). The reason is that extrapolation of a distribution will allow more chance for cancellation of the oscillatory terms in Q_e and G, which are neglected in derivation of (20). Thus, the numerical results suggest that cloud extinction coefficients can be inferred from measurement of the backscatter coefficients directly from (20) without need to know details of the cloud droplet size distribution. If knowledge of the droplet size distribution is available, then extinction coefficients could be determined more accurately by employing the better approximation (16).

The simple linear extinction-backscatter relation (20) should be particularly useful for lidar probing of cloud edges, where entrainment causes intense evaporation and severe distortion of the droplet spectra and where, as a result the spectra, may not be representative of the entire cloud. The associated wide spatial and temporal variability in the droplet spectra will not prohibit the use of our relation (20) to infer extinction coefficients from lidar backscatter coefficients since the relation is size distribution independent.

Of course, backscatter coefficients within cloud can be determined from lidar return signals only so far as radiation from the transmitter can penetrate the cloud and further be backscattered with sufficient intensity so as to be detectable by the receiver. This penetration depth is on the order of several tens of meters for heavy cloud having liquid water content of a few tenths of a gram per cubic meter. Probing the interior of clouds has, in addition to the limitations posed by loss of signal due to attenuation, complications arising from multiple scattering contributions to the lidar return. Monte Carlo calculations of *Kunkel and Weinman* [1976] and *Platt* [1981] show these contributions are appreciable for cloud optical depths greater than about 0.5, depending on the solid angle subtended by the lidar receiver. It is beyond the scope of this paper to discuss methods for taking multiple scattering contributions into account. We only point out there are complications in the interpretation of lidar data that cannot be overcome simply by using knowledge of our relation between backscatter and extinction (20). On the other hand, this relation should simplify the interpretation of lidar data, even when multiple scattering contributions to the lidar return signal are important.

7. Experimental Verification of the Extinction-Backscatter Relation

It would be desirable to compare the extinction-backscatter relation (20) to direct measurements of these quantities. The only known simultaneous measurements of backscatter and extinction in atmospheric cloud are by *Curcio and Knestrick* [1958]. They found empirically a proportionality between extinction and backscatter coefficients of the form $\sigma_e \sim \sigma_b^{0.64}$ for weather conditions including fog, fog and drizzle, and clear weather. However, there is considerable leeway in determining the exponent in this proportionality from their measured data (their Figure 4). In addition, the effects of fog inhomogeneities and multiple scattering contributions to both the backscatter and the transmission signals are potential uncertainties in comparing our relation (20) with their data.

In an attempt to determine experimentally the accuracy of the extinction-backscatter relation (20) we decided to restrict our study to laboratory simulations of cloud (because of the difficulty in making atmospheric measurements). We generated in a cubical 1.0 m^3 chamber polydispersions of cloud droplets using 'cool-mist' vaporizers and a De Vilbiss model 65 ultrasonic nebulizer. Chamber saturation and cloud stability was maintained by soaking a black matt cloth lining the chamber floor with water. The matt cloth also served to reduce stray light levels. Droplet distributions obtained with these generation schemes were generally unimodal (Figure 5) with a range of drop sizes characteristic of clouds. Interestingly, the nebulizer distributions were narrower than those for the cool-mist vaporizers, but they resulted in higher backscatter and extinction levels because of their much higher number concentrations.

Backscatter and extinction measurements were made simultaneously on the laboratory simulated clouds employing a 5.4 mw He-Ne laser source, a synchronous radiometer (Laser Pre-

ission Corporation model Rk 5100) for monitoring laser power, a pyroelectric detector (LPC model RkP-545), for measuring transmitted laser power, and a silicon photodetector (United Detector Technology model PIL-100V) for measuring backscattered light. Measurement of the backscattered light was facilitated with a highly reflective (> 99.3%) circular mirror judiciously positioned on the axis of the laser beam so that a small (3.16 mm) hole drilled through its center would admit the laser beam into the fog chamber, and at the same time intercept light scattered in the near-backward direction. The mirror was tilted about 9° (from the laser beam direction) to reflect the backscattered radiation onto the photodetector. Precautions were taken to ensure that detector aperatures were small enough that forward scattering corrections to both transmission and backscatter signals [*Deepak and Box*, 1978] could be neglected.

The results of these measurements are summarized in Figure 6 where the ratio of extinction to backscatter coefficients at the He-Ne wavelength $\lambda = 0.6328$ μm is within 20% of that predicted by our size-distribution-independent relation (20) for clouds with liquid water contents ranging from 0.05 to 1.0 g m^{-3}. (In this comparison we have used $g(\lambda = 0.6943$ μm$) = 1.42$ rather than a value of g for $\lambda = 0.6328$ μm, but the difference is estimated to be small.) Agreement between experiment and theory is best for polydispersions of droplets having a broad range of sizes (these correspond to data points in Figure 6 where $\sigma_b < 30$ km^{-1} sr^{-1}). The reason for this can be understood by examining the more exact backscatter-extinction relation (17). For broad distributions the higher-order terms in (17) tend to cancel since they are of opposite sign and of comparable magnitudes, making the zero-order approximation (20) a good one. For clouds (generated with the nebulizer technique) having a narrow distribution of smaller droplets (corresponding to data points where $\sigma_b > 30$ km^{-1} sr^{-1}) the agreement between experiment and theory is not quite as good. For these distributions our neglect of the oscillatory contributions to the extinction and backscatter efficiencies render the linear (zero order) relation (20) less accurate.

Nonetheless, it is noteworthy that our measurements of extinction and backscatter are in overall better agreement with theory (relation (20)) than our numerical results in section 6, which are based on measured atmospheric cloud droplet distributions. Part of the explanation for this finding has to do with the limited scope of our laboratory studies. While we tried to generate droplet distributions characteristic of atmospheric cloud, the range of size distributions was nowhere near that for those used in the numerical study. Had we been able to generate larger droplets and narrower distributions in the laboratory, no doubt the agreement between measurements and the linear backscatter-extinction relation (20) would not have been as good.

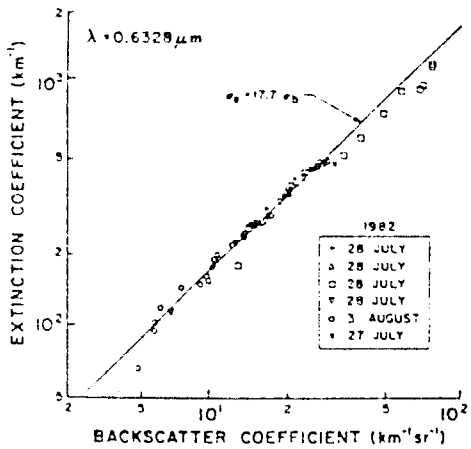

Fig. 6. Comparison of measured cloud backscatter and extinction coefficients (points) with the theoretical relation (20). The backscatter and extinction coefficient measurements were made on laboratory-generated clouds having a variety of size distributions (two examples of which are shown in Figure 5) and liquid contents ranging from 0.05 to 1.0 g m^{-3}. Clouds corresponding to the square data points were generated with the ultrasonic nebulizer technique; all others were generated with cool-mist vaporizers.

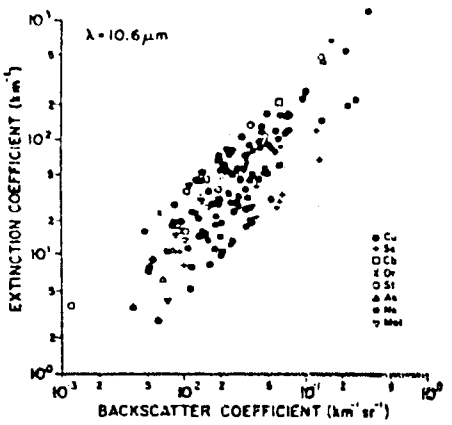

Fig. 7. Same as Figure 4 except for the CO_2 laser wavelength $\lambda = 10.6$ μm. At this longer wavelength the extinction is no longer approximately related to backscatter, as the extinction coefficient for a particular backscatter coefficient varies by about an order of magnitude with the droplet size distribution.

8. Extinction and Backscatter at Middle Infrared and Millimeter Wavelengths

We should not necessarily expect the extinction-backscatter relation (20) for cloud to be applicable at all wavelengths, since the backscatter gain cannot generally be well approximated by slowly varying functions of size parameter at all wavelengths. To prove this conjecture, we calculated the extinction and backscatter coefficients for the previously mentioned 156 cloud size distributions at several laser wave-

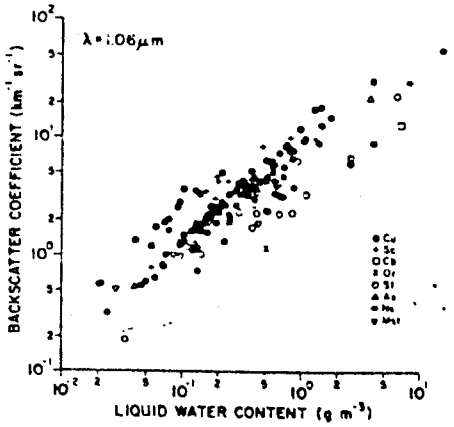

Fig. 8. Volume backscatter coefficient at a wavelength $\lambda = 1.06$ μm versus liquid water content for 156 measured droplet size distributions of cumulus and stratus type clouds. The results show cloud liquid water content is not uniquely related to the backscatter coefficient irrespective of cloud type.

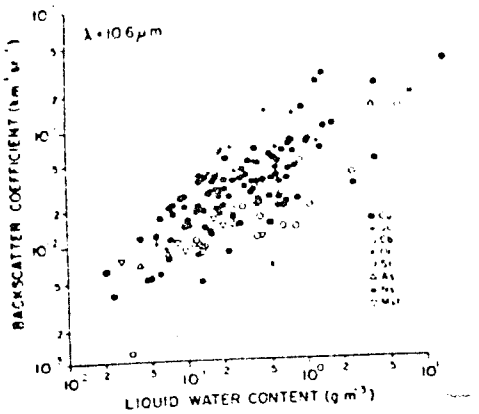

Fig. 9. Same as Figure 8, except for $\lambda = 10.6$ μm.

lengths. An example of the results at the CO_2 laser wavelength $\lambda = 10.6$ μm (Figure 7) show that for a particular backscatter coefficient the extinction varies by an order of magnitude for different size distributions of droplets. (Our neglect of gaseous absorption, which is at most 0.4 km^{-1} at this wavelength, does not significantly affect the results in Figure 7.) Therefore, a CO_2 lidar measurement could not be used (by itself, without constraints on spatial variability of drop size distributions) to deduce infrared ($\lambda = 10.6$ μm) extinction in cloud. (As an aside we note that if the form of the distribution of droplets is spatially invariant the method of *Klett* [1980] can be used to infer extinction profiles from backscatter measurements, regardless of the particular form of the distribution.)

Neither can an approximate extinction-backscatter relation be expected to hold at millimeter wavelengths as can be seen from examining (1) and (2), knowing that the Rayleigh approximation holds for which $G(x) \sim x^4$ and $Q_e(x) \sim x$. Our numerical results based on the 156 drop distributions (not shown here) bear out this conclusion.

9. Backscatter and Liquid Water Content in Cloud

Having been encouraged by the success of the extinction-backscatter relation (20) at visible and near-infrared wavelengths, we extended our investigation to see if a similar relation might exist between cloud liquid water content and backscatter coefficient; the motivation of course being the prospect of utilizing lidar for remote measurement of cloud liquid water content.

The liquid water content W of cloud with droplet size distribution $n(r)$ is given by

$$W = \rho \int \frac{4\pi}{3} r^3 n(r)\, dr \tag{21}$$

where ρ is the density of water.

We already know the backscatter gain for polydispersions of droplets at visible and near-IR wavelengths can be approximated by $G(x) = g(1 + \delta x^2)$. Hence, there can be no size-distribution-independent relation between liquid water content and backscatter coefficient at this wavelength as the ratio of these quantities (after expanding in powers of δ),

$$\frac{W}{\sigma_b} = \frac{16\pi\rho}{3g}\left[\frac{\langle r^3\rangle}{\langle r^2\rangle} - \delta k^2 \frac{\langle r^4\rangle\langle r^3\rangle}{\langle r^2\rangle\langle r^2\rangle} + O(\delta^2)\right] \tag{22}$$

contains in the leading term the ratio of the third to second moments of the droplet size distribution. In other words, at $\lambda = 1.06$ μm the liquid water content of cloud is related to the backscatter coefficient only through a parameter that depends on droplet size distribution. To obtain a quantitative measure of this size distribution dependence, we again performed Mie calculations of the backscatter coefficient by using equation (2) and the liquid water content by using equation (21) for the previously mentioned 156 cloud size distributions. The results are presented in Figure 8 and show that for a particular backscatter coefficient the cloud liquid water content can vary by more than a factor of 10 with the droplet size distribution.

Similar investigations of a possible relation between cloud liquid water content and backscatter coefficient at other infrared, visible, and near-millimeter laser wavelengths $\lambda = 0.55$, 0.694, 3.8, 10.6, 1364 μm (220 GHz), 2143 μm (140 GHz), and 3192 μm (94 GHz) show again that no unambiguous relations exist; and further that for a fixed backscatter coefficient at these other wavelengths the cloud liquid water content is generally an even more sensitive function of the droplet size distribution. An example of these results at $\lambda = 10.6$ μm is shown in Figure 9.

We can, therefore, conclude that for cloud with droplets of unknown size distribution a determination of liquid water content cannot be made solely from a single-wavelength lidar measurement.

10. Extinction and Liquid Water Content in Cloud

It has previously been shown theoretically and verified numerically [*Chýlek*, 1978; *Pinnick et al.*, 1979] that approximate relationships exist between infrared extinction (around $\lambda = 11$ μm) and liquid water content of fogs, and between infrared absorption (around $\lambda = 3.8$ μm, 9.5 μm) and liquid water content of fogs. The relationships are linear of the form

$$\sigma_e = \frac{3\pi c}{2\lambda\rho} W \tag{23}$$

$$\sigma_a = \frac{3\pi c'}{2\lambda\rho} W \tag{24}$$

where σ_e and σ_a are the extinction and absorption coefficients at the wavelength λ, W the fog liquid water content, and the parameters c and c' are equal to the slopes of straight lines that approximate the Mie extinction and absorption efficiency curves by $Q_e(x, \lambda) = c(\lambda)x$ and $Q_a(x, \lambda) = c'(\lambda)x$. The $\sigma_e - W$ relation has been verified experimentally for laboratory-

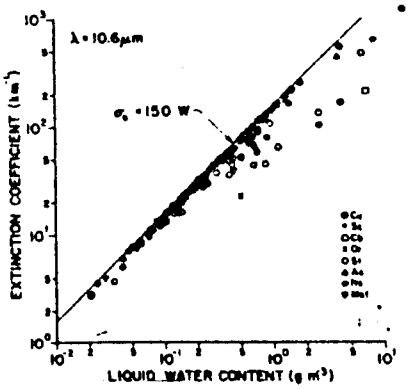

Fig. 10. Volume extinction coefficient at a wavelength $\lambda = 10.6$ μm versus liquid water content for 156 cloud droplet size distribution measurements of cumulus and stratus clouds. Except for cumulonimbus, nimbostratus, cumulus congestus, orographic, and some stratus cloud types the results are close to the equation (23) prediction (shown by the straight line) relating infrared extinction coefficient to liquid water content.

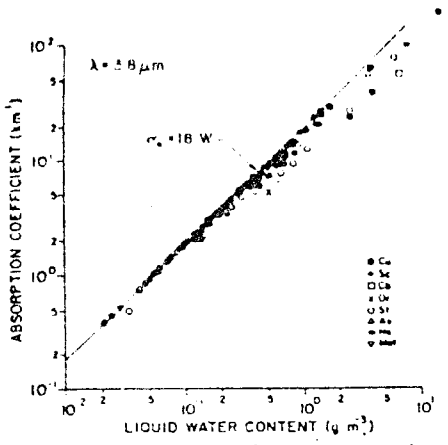

Fig. 11. Volume absorption coefficient at a wavelength $\lambda = 3.8$ μm versus liquid water content for 156 cloud droplet size distributions of cumulus and stratus clouds. For most cloud types the results are close to the equation (24) prediction (shown by the straight line) relating cloud infrared absorption unambiguously to cloud liquid water content.

generated fogs by *Gertler and Steele* [1980] and *Bruce et al.* [1980]. The success of relations (23) and (24) depend on the fact that fog droplets have radii predominately less than $r \cong 14$ μm [*Chýlek*, 1978; *Pinnick et al.*, 1979].

Cloud droplets of course can be much larger than those in fog. For this reason we might not expect relations (23) and (24) to be applicable to all clouds, particularly if droplets with radius $r > 14$ μm dominate either extinction, absorption, or liquid water content. To investigate quantitatively the magnitude of the error involved in the application of (23) and (24) to clouds, we again made Mie calculations of the extinction and absorption coefficients and the liquid water content for the previously considered 156 cloud droplet size distributions summarized in Table 2. The results of these calculations are compared to the size-distribution-independent predictions (23) and (24) in Figures 10 and 11. (The effect of gaseous absorption is small and has been neglected.) Except for cumulonimbus, nimbostratus, cumulus congestus, orographic, and some stratus type clouds [which contain significant number of large ($r > 14$ μm) droplets] the relations (23) and (24) are within a factor of 2 of the numerical results. This comparison thus reaffirms the conclusion of *Chýlek* [1978] that at $\lambda \cong 11$ μm there exists a nearly unique relation betwen extinction coefficient and liquid water content of the form of (23) for nonprecipitating clouds. It also suggests the absorption-liquid content relation (24) can be applied to most clouds without regard to their type or character of their droplet size distribution.

11. Conclusion

For all types of atmospheric clouds consisting of spherical water droplets, an approximate relation between their extinction and backscatter coefficients at visible and near-infrared wavelengths has been derived. To zero order the relation is independent of cloud droplet size distribution. The relation should enable the determination of cloud extinction coefficient (or total droplet surface area) solely from lidar return signals, providing the contribution of multiply-scattered photons to the lidar return can be neglected. However, no size-distribution-independent relation exists between cloud liquid water content and backscatter coefficient at visible, infrared, or near-millimeter wavelengths, suggesting that single-wavelength lidar (by itself) cannot be used to remotely measure cloud liquid water content for clouds of unknown type.

Acknowledgments. One of the authors (P.C.) was supported in part by a U.S. Army Reserve grant DAAG29-80-C-0108.

References

Abramowitz, M., and I. A. Stegun, *Handbook of Mathematical Functions*, National Bureau of Standards, Washington, D. C., 1966.

aufm Kampe, H. J., and H. K. Weickmann, Trabert's formula and the determination of the water content in clouds, *J. Meteorol.*, *9*, 167–171, 1952.

Battan, L. J., and C. H. Reitan, *Artificial Stimulation of Rain*, pp. 184–191, Pergamon, New York, 1957.

Bruce, D., C. W. Bruce, Y. P. Lee, L. Cahenzli, and H. Burket, Experimentally determined relationship between extinction coefficients and liquid water content, *Appl. Opt.*, *19*, 3355–3360, 1980.

Chýlek, P., Extinction and liquid water content of fogs and clouds, *J. Atmos. Sci.*, *35*, 296–300, 1978.

Collis, R. T. H., Lidar observations of cloud, *Science*, *149*, 978–981, 1965.

Curcio, J. A., and G. L. Knestrick, Correlation of atmospheric transmission with backscattering, *J. Opt. Soc. Am.*, *48*, 686–689, 1958.

Deepak, A., and M. A. Box, Forwardscattering corrections for optical extinction measurements in aerosol media, *Appl. Opt.*, *17*, 2900–2907, 1978.

Derr, V. E., Estimation of the extinction coefficient of clouds from multiwave-length lidar backscatter measurements, *Appl. Opt.*, *14*, 2310–2314, 1980.

Derr, V. E., N. L. Abshire, R. E. Cupp, and G. T. McNice, Depolarization of lidar returns from Virga and source cloud, *J. Appl. Meteorol.*, *15*, 1200–1203, 1976.

Diem, M., Messung der Grose con Wolken-elementen, *Meteor. Rudsch.*, *9*, 261–273, 1948.

Diermendjian, D., *Electromagnetic Scattering on Spherical Polydispersions*, American Elsevier, New York, 1969.

Diermendjian, D., Far-infrared and submillimeter wave attenuation by clouds and rain, *J. Appl. Meteorol.*, *14*, 1584–1593, 1975.

Durbin, W. G., Droplet sampling in cumulus clouds, *Q. J. R. Meteorol. Soc.*, *11*, 202–215, 1959.

Eagan, R. C., P. V. Hobbs, and L. F. Radke, Particle emissions from a large Kraft mill and their effects on the microstructure of warm clouds, *J. Appl. Meteorol.*, *13*, 535–552, 1974.

Fitzgerald, J. W., A study of the initial phase of cloud droplet growth by condensation: Comparison between theory and observation, Ph.D. Dissertation, Univ. of Chicago, Ill., 1972.

Fitzgerald, J. W., and P. A. Spyers-Duran, Changes in cloud nucleus concentration and cloud droplet size distribution associated with pollution from St. Louis, *J. Appl. Meteorol.*, *12*, 511–516, 1973.

Gertler, A. W., and R. L. Steele, Experimental verification of the linear relationship between IR extinction and liquid water content of clouds, *J. Appl. Meteorol.*, *19*, 1314–1317, 1980.

Hale, G. M., and M. R. Querry, Optical constants of water in the 200 nm to 20 μm wavelength region, *Appl. Opt.*, *12*, 555–563, 1973.

Jiusto, J. E., Aerosol and microphysics measurements in Hawaii, *Tellus*, *19*, 359–368, 1967.

Khare, V., Short-wavelength scattering of electromagnetic waves by a homogeneous dielectric sphere, PhD Thesis, Univ. of Rochester, Rochester, New York, 1976.

Khare, V., and H. M. Nussenzveig, Theory of the glory, *Phys. Rev. Lett.*, *38*, 1279–1282, 1977*a*.

Khare, V., and H. M. Nussenzveig, The theory of the glory, in *Statistical Mechanics and Statistical Methods in Theory and Application*, edited by Uzi Landman, Plenum, New York, 1977*b*.

Klett, J. D., Stable analytical inversion solution for processing lidar returns, *Appl. Opt.*, *20*, 211–220, 1981.

Kunkel, K. E., and J. A. Weinman, Monte Carlo analysis of multiply scattered lidar returns, *J. Atmos. Sci.*, *33*, 1772–1781, 1976.

Nussenzveig, H. M., High-frequency scattering by a transparent sphere, 2, Theory of the rainbow and glory, *J. Math. Phys.*, *10*, 125–176, 1969.

Nussenzveig, H. M., Complex angular momentum theory of the rainbow and the glory, *J. Opt. Soc. Am.*, *69*, 1068–1079, 1979.

Nussenzveig, H. M., and W. J. Wiscombe, Efficiency factors in Mie scattering, *Phys. R...*

Pinnick, R. G., and H. J. Auvermann, Response characteristics of Knollenberg light-scattering aerosol counters, *J. Aerosol. Sci.*, *10*, 55–74, 1979.

Pinnick, R. G., S. G. Jennings, P. Chýlek, and H. J. Auvermann, Verification of a linear relation between IR extinction, absorption and liquid water content of fogs, *J. Atmos. Sci.*, *36*, 1577–1586, 1979.

Plass, G. N., and G. W. Kattawar, Reflection of light pulses from clouds, *Appl. Opt.*, *10*, 2304–2310, 1971.

Platt, C. M. R., Lidar and radiometric observation of cirrus clouds, *J. Atmos. Sci.*, *30*, 1191–1204, 1973.

Platt, C. M. R., Remote sounding of high clouds, 3, Monte Carlo calculations of multiple-scattered lidar returns, *J. Atmos. Sci.*, *38*, 156–167, 1981.

Ryan, R. T., H. H. Blau, P. C. von Thuna, and M. L. Cohen, Cloud microstructure as determined by an optical cloud particle spectrometer, *J. Appl. Meteorol.*, *11*, 149–156, 1972.

Schotland, R. M., K. Sassen, and R. Stone, Observation by lidar of linear depolarization ratios for hydrometeors, *J. Appl. Meteorol.*, *10*, 1011–1017, 1971.

Shipley, S. T., and J. A. Weinman, A numerical study of scattering by large dielectric spheres, *J. Opt. Soc. Am.*, *68*, 130–134, 1978.

Silverman, B. A., and E. Sprague, Airborne measurement of in-cloud visibility, paper presented at Proceedings of the Second National Conference on Weather Modification, Am. Meteorol. Soc., Santa Barbara, California, April 6–9, 1970.

Singleton, F., and D. J. Smith, Some observations of drop size distributions in low layer clouds, *Q. J. R. Meteorol. Soc.*, *86*, 458–467, 1960.

Spyers-Duran, P. A., Systematic measurements of cloud particle spectra in middle level clouds, *Tech. Note 43*, Cloud Physics Lab., Univ. of Chicago, Chicago, Ill., 1972.

Squires, P., The microstructure and colloidal stability of warm clouds, 1, The relation between structure and stability, *Tellus*, *10*, 256–261, 1958.

Twomey, S., and H. B. Howell, The relative merit of white and monochromatic light for the determination of visibility by backscattering measurements, *Appl. Opt.*, *4*, 501–506, 1965.

Vogt, H., Visibility measurement using backscattered light, *J. Atmos. Sci.*, *25*, 912–918, 1968.

Warner, J., The microstructure of cumulus cloud, 1, General features of the droplet spectrum, *J. Atmos. Sci.*, *26*, 1049–1059, 1969.

Warner, J., The microstructure of cumulus cloud, 4, The effect of the droplet spectrum of mixing between cloud and environment, *J. Atmos. Sci.*, *30*, 256–261, 1973*a*.

Warner, J., The microstructure of cumulus cloud, 5, Changes in droplet size distribution with cloud age, *J. Atmos. Sci.*, *30*, 1724–1726, 1973*b*.

Weickmann, H. K., and H. J. aufm Kampe, Physical properties of cumulus clouds, *J. Meteorol.*, *10*, 204–211, 1953.

Zuev, V. E., and Yu. S. Balin, Investigation of atmospheric boundary layers and clouds by the laser tracking method, *Fizika*, *15*, 125–128, 1972.

(Received November 29, 1982;
revised April 25, 1983;
accepted April 27, 1983.)

APPENDIX 2

Extinction and Liquid Water Content of Fog at Visible Wavelengths.

S.G. Jennings

Applied Optics, 22, pp. 2514-2515, 1983.

Reprinted from **Applied Optics**, Vol. 22, page 2514, September 1, 1983

Extinction and liquid water content of fog at visible wavelengths

S. G. Jennings

University College, Physics Department, Galway, Ireland.

Received 24 March 1983.
0003-6935/83/172514-02$01.00/0.

Recently, Lenham and Clay[1] obtained high correlation for a linear relationship between a measured extinction coefficient in fog at wavelength $\lambda = 0.53\ \mu m$ and liquid water content. The liquid water content values were derived from number-size distribution histograms, which in turn were inferred from transmission measurements at several wavelengths using an inversion algorithm.[2] They also found a high correlation between the inferred number concentration in the largest size category (6.4–12.8-μm radius) and the extinction coefficient.

The purpose of this Letter is to point out that high correlation between visible extinction and liquid water content for fog cannot be expected to hold in general. In addition, the correlation of number concentration with extinction is examined, and the conclusion is drawn that it is very unlikely in general for extinction to be linearly related to number concentration for fog size distributions at visible wavelengths.

The volume extinction coefficient σ_e is given by

$$\sigma_e = \int_0^\infty \sigma_{ext}(m,x)n(r)dr, \tag{1}$$

where $n(r)$ is the droplet size distribution. The single-particle extinction cross section $\sigma_{ext}(m,x)$ is a function of the droplet complex index of refraction m and the size parameter $x = 2\pi r/\lambda$, the ratio of the droplet circumference to the wavelength λ.

Chýlek[3] has shown that the extinction σ_e is linearly related to liquid water content W by

$$\sigma_e = \frac{3\pi c}{2\rho\lambda} W, \tag{2}$$

where ρ is the density of water, and the coefficient c is equal to the slope of a straight line that approximates the normalized extinction cross section $Q_{ext}(m,x)$ by

$$Q_{ext}(m,x) = c(m)x \tag{3}$$

Chýlek[3] has shown that for $\lambda = 0.5\ \mu m$, Q_{ext} is proportional to x with $c = 0.61$ providing fog droplets have a size parameter of <0.5. A similar result is obtained here for $\lambda = 0.53\ \mu m$ (used by Lenham and Clay[1]). This corresponds to a maximum allowable radius of $0.55\ \mu m$ if a linear relationship between extinction and liquid water content (LWC) is to hold independent of size distribution. It is clear since the fog droplet size distributions of Lenham and Clay[1] possess radii greatly in excess of $0.55\ \mu m$ that no unique relation should exist between extinction and LWC at visible wavelengths. This result also applies to fog size distributions in general.

Table I. Mean Extinction Cross Sections per Droplet for the Listed Channel Widths at Wavelength 0.53-μm; Index of Refraction m: 1.3338–1.45×10^{-9}

Channel	Radius interval (μm)	Mean extinction cross section per particle (cm^2)
1	0.2–0.4	7.655×10^{-9}
2	0.4–0.8	3.859×10^{-8}
3	0.8–1.6	1.131×10^{-7}
4	1.6–3.2	4.180×10^{-7}
5	3.2–6.4	1.603×10^{-6}
6	6.4–12.8	6.254×10^{-6}
	12.8–25.6	2.464×10^{-5}

A Mie scattering code which incorporates Wiscombe's[4] recent algorithms is used to compute the mean extinction cross sections per particle for the histogram channel widths used by Lenham and Clay[1] and for an additional channel width of 12.8–25.6 μm. The interpolated value of the complex refractive index of water[5] at $\lambda = 0.53\ \mu m$ was used. The computed mean extinction cross sections are given in Table I. The contribution to the extinction coefficient by an individual channel is obtained from the product of mean extinction cross section and droplet number concentration of that channel (assuming the number distribution is uniform over the channel).

The mean extinction cross section increases approximately as the square of the radius for a large size parameter, as can be seen in Table I for the last four radius intervals. For an equal number concentration of cm^{-3} over their radius intervals, channel 6 dominates (76% contribution) the extinction from these channels. An examination of the differential number concentration of $cm^{-3}\ \mu m^{-1}$ for the three largest size intervals (4, 5, and 6 in Table I) in Fig. 2 of Lenham and Clay[1] reveals that the total extinction is dominated by the contribution from the largest size interval (6.4–12.8 μm). For example, at time 21.40 the 6.4–12.8-μm channel contributes over 80% of total extinction. Therefore, it is not surprising to find a strong correlation between extinction and LWC for the 6.4–12.8-μm interval of Lenham and Clay[1] since the channel dominates both extinction and liquid water content.

Moreover the inversion scheme[2] used by Lenham and Clay[1] truncates the size distribution spectrum at 12.8-μm radius. There is strong evidence[6–8] that both radiation and advection fogs possess radii in excess of 12.8 μm. The contribution of a seventh channel (12.8–25.6 μm) to total extinction would amount to more than 10% allowing for a plausible order of magnitude drop in concentration cm^{-3} from that of channel 6. This would grossly alter the form of the histogram deduced by Lenham and Clay,[1] and it would also weaken the high correlation between visible extinction and liquid water content obtained by Lenham and Clay.[1]

The relationship between calculated extinction and LWC based on measured fog size distributions for radiation and

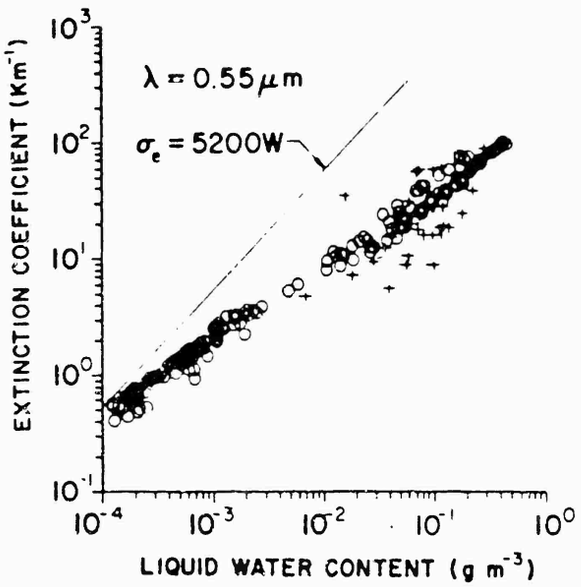

Fig. 1. Variation of extinction coefficient with liquid water content in atmospheric fog and haze for 320 size distribution measurements made at different geographic locales and under a variety of meteorological conditions as shown by Pinnick *et al.*[8]

advection fog at $\lambda = 0.55\ \mu m$ has been shown[8] not to be unique. Indeed extinction can vary by approximately an order of magnitude for a particular LWC value as shown by Pinnick *et al.*[8] and reproduced in Fig. 1.

The correlation of number concentration with extinction was examined by Lenham and Clay.[1] In general, they found a weak correlation between number concentration and extinction with the exception of the 6.4–12.8-μm category for a dense fog. However, a study of inferred droplet concentration for the 6.4–12.8-μm category and extinction at $\lambda = 0.53\ \mu m$ for the four fog case studies of their Fig. 1 reveals that a strong correlation does not exist between number concentration and extinction. It is clear from Eq. (1) that extinction will be linearly related to number concentration only if extinction cross section σ_{ext} and size distribution $n(r)$ vary with droplet size over the whole size range in an inverse manner. For example, if σ_{ext} varies as r^2, extinction will vary linearly with number concentration only if $n(r)$ varies as $1/r^2$. The above conditions on σ_{ext} and $n(r)$ are unlikely to be met over a typical fog droplet size distribution in view of (a) the characteristic resonance response of σ_{ext} to size and (b) the widespread evidence[6–8] that many fog droplet size distributions are bimodal in character. Thus, in general, it is extremely unlikely that extinction will be linearly related to number concentration for a fog size distribution spectrum at visible wavelengths.

This work was supported by means of a research contract with the U.S. Army through its European Research Office, London.

References

1. A. P. Lenham and M. R. Clay, Appl. Opt. **21**, 4191 (1982).
2. J. Heintzenberg, H. Mueller, H. Quenzel, and E. Thomalla, Appl. Opt. **20**, 1308 (1981).
3. Petr Chýlek, J. Atmos. Sci. **35**, 296 (1978).
4. W. J. Wiscombe, Appl. Opt. **19**, 1505 (1980).
5. G. M. Hale and M. R. Querry, Appl. Opt. **12**, 555 (1973).
6. J. A. Garland, Q. J. R. Meteorol. Soc. **97**, 483 (1971).
7. R. J. Pilié, E. J. Mack, W. C. Kocmond, W. J. Eadie, and C. W. Rogers, J. Appl. Meteorol. **14**, 364 (1975).
8. R. G. Pinnick, S. G. Jennings, P. Chýlek, and H. J. Auvermann, J. Atmos. Sci. **36**, 1577 (1979).